EFFECTS OF EXOSKELETON WALKING THERAPY IN THE DISTAL FEMUR AND PROXIMAL TIBIA IN INDIVIDUALS WITH CHRONIC SPINAL CORD INJURY

by

Nicole Mattson

A Thesis

Submitted to the Faculty

of the

WORCESTER POLYTECHNIC INSTITUTE

in partial fulfillment of the requirements for the

Degree of Master of Science

in

Biomedical Engineering

May 2021

Approved:

Dr. Karen L. Troy, Thesis Advisor: _____

Dr. Adam Lammert, Committee member: _____

Dr. Leslie Morse, Committee member: _____

Acknowledgements

Thank you to my advisor Dr. Karen Troy, for welcoming me into the lab in uncertain times and allowing me to work on this project. Without your guidance and willingness to help with anything I needed, this project would not have been possible. I would also like to thank my committee members, Dr. Adam Lammert and Dr. Leslie Morse, for being a part of this project and giving important feedback along the way.

I also want to thank everyone associated with the clinical trial (NCT02533713) this project was associated with including Ricardo Battaglino, Nguyen Nguyen, Candy Tefertiller as well as the physical therapists at Craig Hospital and the research participants for taking part in the clinical trial associated with this project. Everyone's hard work and dedication to this study should not go unrecognized. This research was funded by W81XWH-15-2-0078 (to LRM).

Thank you to all of my family and friends for supporting me throughout this entire process.

Contents

Table of Figures:

Table of Tables:

List of Abbreviations:

SCI:	Spinal cord injury
CT:	Computed tomography
AIS:	Association impairment scale
BMD:	Bone mineral density
BMC:	Bone mineral content
DXA:	Dual-energy X-ray absorptiometry
FES:	Functional electrical stimulation
PTH:	Parathyroid hormone
COP:	Center of pressure
aBMD:	Areal bone mineral density
QCT:	Quantitative computed tomography
CSA:	Cross-sectional area
CSI:	Compressive strength index
BSI:	Bending strength index
BR:	Buckling ratio
iBMC:	Integral bone mineral content
BV:	Bone volume
ROI:	Region of interest
BPAQ:	Bone specific physical activity questionnaire
BLHQ:	Bone loading history questionnaire
GRF:	Ground reaction force

Abstract

Background

More than 294,000 people in the United States are living with spinal cord injuries, and over 17,000 new injuries occur every year. Individuals with SCI experience a sudden decrease in mechanical loading in their lower limbs, leading to severe bone loss known as SCI-induced osteoporosis. One proposed method to treat SCI-induced bone loss is to use exoskeleton walking therapy to load the lower limbs, but it is currently unknown whether or not the loading experienced is sufficient for any therapeutic benefits. An ongoing clinical trial (NCT 02533713) associated with this thesis allows 30 individuals with chronic SCI to complete exoskeleton walking therapy for six months. We hypothesized that exoskeleton walking therapy would be sufficient to provide therapeutic benefit, resulting in a significant increase in the bone mineral content (BMC; g) in the distal femur and proximal tibia. We also proposed to assess the kinetics and kinematics associated with walking therapy for each participant. Finally, we hypothesized that there would be a positive relationship between the change in BMC and a participant-specific measure of "bone loading dose". Thus, our overall purpose was to determine the degree to which exoskeleton walking therapy influences BMC in a dose-dependent manner.

Methods

The present analysis includes data from 13 participants in the clinical trial. Computed tomography (CT) scans including at least 15 cm of the distal femur and proximal tibia were taken before and after six months of exoskeleton walking therapy. The scans were analyzed quantitatively (quantitative computed tomography; QCT) to calculate BMC and participant-specific measures of bone strength. The bone strength measures were used to create candidate loading dose calculations for each participant. The clinical trial intervention included 6 months of exoskeleton walking therapy performed 3 hours a week, using either the EKSO or Indego exoskeleton. Video data and pressure sensing insole data was captured during the final walking therapy sessions. The data were used to calculate the kinetics and kinematics for each individual while walking in the exoskeleton. The exoskeleton recorded the number of steps each user took and the

pressure sensing insoles provided the magnitude and location of the center of pressure over time, which were also used to calculate candidate measures of loading dose. We used paired t-tests to compare pre- versus post-intervention values of BMC. We also used independent t-tests to compare the kinetics and kinematics of walking between the two exoskeletons. Finally, Pearson's correlations were calculated to assess the relationship between the changes in BMC and the various loading dose calculations.

Results

There was a significant 2.40 ± 4.83% increase in femur BMC following exoskeleton walking therapy ($p = 0.038$). There was also a significant 8.34 ± 11.60 % and 4.23 ± 9.80 % increase in BMC of the epiphyseal region of the femur and tibia respectively ($p \leq 0.023$). The kinematics and temporal parameters varied between the two exoskeletons, with the Indego having a higher range of motion at the knee and ankle, and a faster stride time and walking speed than the EKSO. Loading dose was more closely associated with change in femur BMC versus tibia BMC (tibia $r = -0.048$ to -0.143, versus femur $r = 0.265$ to 0.457). Change in femur BMC was most positively correlated with loading dose calculated using the femoral epiphyseal bending strength index ($r=0.457$, $p=0.024$).

Conclusion

BMC increased in regions of the distal femur and proximal tibia following exoskeleton walking therapy. The kinematics and kinetics between the Indego and EKSO exoskeletons varied, but not enough to have a significant impact on the net joint forces at the ankles and knees of the users. Moderate positive correlations between participant specific loading dose calculations using femur strength metrics suggest that bone changes in a dose-dependent manner as a result of exoskeleton walking therapy. Assessing changes in bone mass compared to the amount of loading during walking therapy can provide important information to identify therapeutic targets and predict response due to exoskeleton walking therapy.

Chapter 1: Introduction

It is estimated that there are 294,000 people in the United States living with SCI, and 17,810 more cases occur each year (National Spinal Cord Injury Statistical Center, 2018). People with SCI experience bone loss in the lower limbs over time following SCI, known as SCI induced osteoporosis (Battaglino et al., 2012; Garland et al., 2001, 2008; Lobos et al., 2018; Leslie R. Morse et al., 2019; Zehnder, Lüthi, et al., 2004). Bone adapts to the amount of loading it experiences and those with SCI experience a drastic reduction in loading following injury (C. H. Turner, 1998). SCI induced osteoporosis puts people with SCI at a higher risk of fracture, up to 50% of those with SCI (Bauman & Cardozo, 2015; S. D. Jiang et al., 2006; Szollar et al., 1997). When an individual with SCI sustains a fracture, he or she is at risk for respiratory infections, pressure ulcers, urinary tract infections, thromboembolic events, depression, and delirium (Carbone et al., 2013a). There are limited options for therapies in individuals with spinal cord injuries. Some options for bone loss treatments include bisphosphonates, antisclerostin antibodies, mechanical and electrical stimulation of the lower extremities, or mechanical stimulation using vibrations (Battaglino et al., 2012).

One way to potentially reverse osteoporotic effects would be to induce mechanical loading on the lower limbs (Battaglino et al., 2012). A unique method of inducing this mechanical loading on lower limbs with people who have an SCI is an exoskeleton (Indego, Parker Hannifin, Cleveland, OH) and EKSO (ekso Bionics, Richmond, CA). Exoskeletons have been used in therapy for individuals with SCI to improve gait function and balance by moving the lower limbs using motors (Baunsgaard et al., 2018). We expect that exoskeleton assisted walking will mechanically stimulate the lower extremities with potential therapeutic effects.

We currently do not understand if exoskeleton walking therapy is beneficial or enough to load bones during walking. It is well known that bone adapts to the magnitude and rate of mechanical stimulation, but exoskeleton therapy is a unique method to apply moments and forces at ankle, knee, and hip joints to load the lower limbs (C. H. Turner, 1998). In the broader clinical setting, mechanical loading

using exoskeletons could improve bone health in many types of patient populations who have trouble with balance, muscle weakness in the legs, and individuals with spinal cord injuries. We also do not know if people with spinal cord injuries will be able to gain bone using the exoskeleton therapy. To understand the answers to these many unknowns, a clinical trial is ongoing (NCT02533713) and involves people with spinal cord injury under 40 years old who are between 3 to 10 years post injury. Baseline data has already been collected on 31 participants, follow-up data has been collected on 20 people, and end of trial data has been collected on 12 people. This clinical trial is a crossover study that lasts one year. Each participant is randomly assigned to either exoskeleton walking therapy or usual care for the first 6 months. The groups are switched for the remainder of the year. Computed tomography (CT) scans are taken at the beginning of the trial, the 6-month mark, and the 12-month mark. Additionally, video data are captured of the individuals using the exoskeleton with fiducial markers at the hip, knee, ankle, heel, and toe. Pressure sensing insoles are also used during the clinical trial and correspond to the video footage of individuals walking in the exoskeleton (Orpyx LogR, Orpyx, Calgary, Alberta, Canada).

One of the main goals of the clinical trial is to identify if exoskeleton assisted walking therapy affects bone strength and structure in the lower paralyzed limbs. The purpose of this project is to quantify changes in the bone mineral content of the distal femur and proximal tibia of the participants during the clinical trial. Additionally, using video and pressure sensing insole data, and the known duration of exoskeleton therapy, an estimation of bone loading dose will be calculated.

Specific Aim 1: Quantify changes in tibia and femur bone volume and bone mineral content before and after exoskeleton therapy

The distal end of the femur and proximal tibia will be isolated in the initial, six month, and final CT scans of clinical trial participants for quantitative analysis. The trabecular and cortical regions of distal femur and proximal tibia will be segmented. The overall bone mineral content will be calculated from these scans using the trabecular and cortical regions.

Specific Aim 2: Calculate net knee joint contact force and moment based on kinematics of exoskeleton therapy videos and pressure sensing insole data

The kinematics of the individuals walking in the exoskeleton will be analyzed and combined with pressure sensing insole data to determine the forces and moments at the knee joint. We will also compare Ekso vs. Indego kinematics and dynamics.

Specific Aim 3: Determine the relationship between candidate measures of "loading dose" and bone mineral content changes.

The forces in the knee will be analyzed over the stance phase of walking and multiplied by the duration of the participants' therapy to calculate various candidate measures of "loading dose". We hypothesize that higher loading dose will be related to improved bone.

Hypothesis:

We hypothesized that exoskeleton therapy will increase participants bone mineral content in the proximal tibia and distal femur. Additionally, we hypothesized that there would be difference in the kinetics and kinematics between the two exoskeletons used in the clinical trial. Finally, we hypothesized that the exoskeleton therapy will increase bone mineral content in individuals in a dose-dependent manner.

Chapter 2: Literature Review

Bone structure and adaptation

The cells that make up bones are important for the normal physiological function and remodeling of bone tissue itself. There are four specific types bone cells that reside within bone tissue: osteoprogenitor cells, osteoblasts, osteoclasts, and osteocytes (Mohamed, 2008; Qiu et al., 2019). Osteoprogenitor cells exist towards the periosteal surface of the bone and derive from differentiated mesenchymal stem cells in the periosteum of the bone (Qiu et al., 2019). These cells act as bone cell precursors and eventually become osteoblasts (Qiu et al., 2019). Osteoblasts exist just below the osteoprogenitor cells, and as they become buried deeper in the matrix of the bone, they become osteocytes (Mohamed, 2008). Osteoclasts, on the other hand, are large multinucleated cells created by the differentiation of hematopoietic progenitor cells in the bone marrow (Bar-Shavit, 2007). Osteoclasts have ruffled edges that release acids and collagenolytic enzymes to resorb bone (Bar-Shavit, 2007). The process of building bone by osteoblasts, and resorbing bone via osteoclasts is a continuous process of bone remodeling.

The most prevalent and long-lasting cells in the bone are osteocytes. Osteocytes make up around 95 % of all bone cells in the body (Franz-Odendaal et al., 2006; Frost, 1960). Lamellae are concentric rings in the osteons, and within those osteons, osteocytes reside in gaps called lacunae (Bonewald, 2007). Osteocytes have dendritic portions that span through small gaps in the bone matrix known as canaliculi (Robling & Bonewald, 2020). Through these connections, osteocytes can send and receive signals from other bone cells and the surrounding bone (Robling & Bonewald, 2020).

It is well understood that bone adapts to mechanical loading. Charles Turner summarized the rules for bone adaptation as follows: bones adapt to dynamic loading and do not necessarily have to be exposed to the loading for a long period of time for changes within the bone to occur, and cells within the bone can also become accustomed to the loading they experience (C. H. Turner, 1998). Even though these rules are well-established, being able to understand a relationship between the exact amount of loading and the bone adaptation that occurs as a result has been the focus of many different studies. The strain that bone

experiences it the driving mechanism for bone adaptation, thus the more strain the bone experience, the more the bone should adapt (C. H. Turner, 1998). Mikić and Carter in 1995 presented an energy equivalent strain equation that could represent the total quantity of strain as a scalar regardless of direction of the applied strain (Mikic & Carter, 1995). They also propose the idea of a daily strain stimulus, which incorporates the total number of independent loading cases and cycles and the equivalent strain for the given action (Mikic & Carter, 1995). Adaptation because of higher levels of strain has been shown in athletic populations, with a study by Faulkner et al. where young female gymnasts had higher axial and bending strength, and higher strength indices compared to non-gymnasts of the same age (Faulkner et al., 2003). Bone remodeling has also occurred as a result of novel loading as demonstrated by St. James and Carroll who performed a meta-analysis of exercise regimens with premenopausal women. They determined that the exercise protocols that incorporated odd or high impact loading resulted in an increase in BMD in the lumbar spine and femoral neck (St. James & Carroll, 2010). More recent research has specifically looked at how loading dose affects bone remodeling in the ultradistal radius in adult women (Troy et al., 2020). After twelve months of loading, they determined that 'loading dose' had a positive correlation with the total change in the ultradistal radius integral bone mineral content (iBMC). The conclusion was that strain rate, and strain magnitude and the number of cycles can contribute to bone remodeling (Troy et al., 2020).

There are different theories as to how mechanical forces are received within the osteocytes. One theory involves fluid gradients through the lacunae and canaliculi that creates shear stresses on the surface of the osteocytes as a result of bone bending. Another theory is that drag forces on the structures that adhere the osteocytes to the canaliculi create strain on the overall osteocyte. There is also the possibility that the spaces in the bone, like the lacunae and canaliculi, amplify the strains on the bone immediately next to the osteocyte, allowing it to sense the strain changes (Robling & Bonewald, 2020). Other evidence suggests that osteocytes have primary cilia that bend and move as a result of fluid flow. This movement may have an influence on the balance between bone resorption and formation (Malone et al., 2007). There is ample evidence for all suggested theories, and Robling and Bonewald propose that osteocytes utilize several of these mechanisms to balance bone remodeling overall (Robling & Bonewald, 2020).

In addition to regulating the response of bone to mechanical activity, osteocytes also have known signaling pathways that dictate osteoclast and osteoblast activity. To regulate the osteoclast activity, osteocytes release RANKL or OPG molecules to either induce cell resorption, or inhibit cell resorption respectively (Nakashima et al., 2011). Osteocytes release numerous signaling factors, but there are two that have the most notable effect on osteoblasts: sclerostin and Dkk1, which are Lrp5/6 antagonists and inhibit the Wnt pathway (Robling et al., 2008). In the Wnt signaling pathway, Wnt, Frizzled, and low-density lipoprotein receptor-related protein (LRP)-5 or LRP-6 create a co-receptor complex that enables β-catenin to enter the nucleus. The β-catenin acts to encourage bone formation via osteoblast differentiation, function, and proliferation (Battaglino et al., 2012). The Wnt pathway is crucial in dictating the level of osteogenic response bone has to mechanical loading (Tu et al., 2012).

Overall, bone remodeling is a carefully coupled mechanism of bone breakdown via osteoclasts and bone build up via osteoblasts. Osteocytes aid in facilitating the signaling to orchestrate these systems as a result of mechanical signals when the bone is loaded. In the case that mechanical loading is removed, the balanced process of bone remodeling and bones ability to become accustomed to loads, can result in less ideal bone.

Spinal cord injury-induced osteoporosis

Spinal cord injuries can vary in their physiological impacts depending on the severity and location of the injury. The American Spinal Injury Association has developed a technique to classify the severity of spinal injuries. The American Spinal Injury Association Impairment Scale (AIS) was designed to characterize spinal cord injuries by performing sensory and motor tests on different mapped regions of the body (Roberts et al., 2017). These tests are each graded and assessed together to determine whether the injury is complete or incomplete. The AIS helps clinicians understand if and what type of recovery is expected in a patient based and how best to approach their therapy. In instances when the spinal cord injury is more severe, the injury can inhibit movement of lower extremities, thus decreasing use and loading on the lower limbs. Given that bones adapt to mechanical loading, as aforementioned, a drastic decrease in

mechanical loading can impact the formation and activity of osteoblasts and osteoclasts, leading to alterations in bone morphology.

It is well documented that in the first few months after injury, bones below the site of injury rapidly demineralize (Garland et al., 2001, 2008; Lobos et al., 2018; Leslie R. Morse et al., 2019). There are two main stages in the bone loss as a result of SCI: rapid acute bone loss, and chronic bone loss at a slower rate (Troy & Morse, 2015). During the acute phase of bone loss, there is a decrease in bone mineral density (BMD) in the trabecular regions of bone and cortical thinning. This bone loss usually plateaus after two years. In the chronic phase, the bone loss is not as well characterized, but it has been shown that the BMD and bone mineral content (BMC) decrease over this phase. Additionally, the average time until fracture is usually nine years post injury, during the chronic bone loss phase (Troy & Morse, 2015). It has also been documented that the greatest observed changes in bone are in weight-bearing and trabecular rich regions like the distal femur and proximal tibia (Maïmoun et al., 2006). In these regions, the microarchitecture of the trabecular bone can begin to erode, resulting in a decrease in BMD (Battaglino et al., 2012; Maïmoun et al., 2006). The decrease in BMD can reach 40% in just two years after injury (Battaglino et al., 2012). In regions of cortical bone, cortical thinning is observed at a much slower and steadier rate than trabecular deterioration. Cortical bone loss is believed to be due to the resorption of the endosteal surface of the bone, particularly in the bone shaft (Edwards et al., 2014). The cortical thinning and loss of BMD in the trabecular regions of the bone contribute to the overall decrease in BMC that can be seen as early as one year following injury (Battaglino et al., 2012; Maïmoun et al., 2006).

Although it is evident that SCI leads to a decrease in BMC, there is debate regarding whether the bone loss plateaus after a number of years post-injury. The years until the bone loss reaches this steady-state is also not consistent among sources, ranging from 2 years, to 3-8 years, or even 19 years post injury (Biering-Sorensen & Schaadt, 1990; Edwards et al., 2015; Eser et al., 2004; Jiang et al., 2006; Szollar et al., 1997) (Edwards et al., 2015; Eser et al., 2004; Jiang et al., 2006; Szollar et al., 1997). Other studies found that the bone loss, specifically in the trabecular regions, had a positive correlation with respect to time since injury (Battaglino et al., 2012).

Regardless of whether the bone loss reaches a steady-state, changes in bone physiology are evident quickly following injury as within a few days. Hypercalciuria, which is indicative of an increase in calcium excretion has been documented in individuals with SCI in levels higher than that of people on bedrest (Biering-Sørensen et al., 2009). This indicates that lack of mechanical loading alone might not be the only aspect of SCI affecting bone physiology. Other factors may include alterations in circulation to the bones, and hormonal changes (Maïmoun et al., 2006).

To better understand how to treat spinal cord injury-induced osteoporosis, it is necessary to assess the physiological changes occurring in the bone as a result of decreased mechanical loads. One signaling pathway that has a direct impact on bone formation is the Wnt pathway, as mentioned in the previous section. When this pathway is blocked by an inhibitor, specifically sclerostin, it can have a significant impact on bone's ability to remodel by decreasing osteoblastic activity and increasing osteoclastic activity. Individuals with SCI experience this elevation in sclerostin initially until 5 years post-injury. Following this period, the amount of sclerostin begins to decline due to there being substantially less bones, and fewer osteocytes able to express sclerostin. This becomes an important measure for bone loss in chronic SCI individuals (Battaglino et al., 2012).

SCI-induced osteoporosis presents itself as a significant decrease in BMD and BMC immediately following injury, lasting many years. The changes in bone physiology are believed to be caused by a decrease in mechanical loading associated with increased osteocyte expression of sclerostin. SCI-induced osteoporosis puts individuals at risk for fractures even without the presence of high impact forces. Those with SCI are 5-23 times more likely to experience fracture than those who are able-bodied of the same age range, which can lead to serious health complications (Troy & Morse, 2015).

Treatments and therapies for bone loss after spinal cord injury

To date, there is no restorative treatment for individuals with complete spinal cord injuries. One of the major goals associated with spinal cord injury treatments is the maintenance and protection of the existing bone and muscle in the areas below the injured region. Such treatments include pharmacological

approaches and physical rehabilitation techniques. One of the pharmacological treatments is the use of bisphosphonates, such as clodronate, alendronate, and zoledronic acid (Bryson & Gourlay, 2009; Soleyman-Jahi et al., 2018). The evidence supporting the use of bisphosphonates to reduce the rate at which BMD decreases varies in quality and quantity. Two notable studies assessed bisphosphonate use in individuals with chronic spinal cord injuries using alendronate (De Brito et al., 2005; Zehnder, Risi, et al., 2004). In the study by Zehnder et al., both chronic and acute SCI individuals (0.1 – 29 post injury) were included. Dual-energy X-ray absorptiometry (DXA) was used to assess the change in BMD at the lumbar spine, total hip, distal forearm, distal tibial diaphysis, distal tibial epiphysis. The study concluded that after 24 months of treatment, there was a significant decrease in BMD loss at the distal tibial epiphysis, diaphysis, and the total hip. In the De Brito et al. study, 19 participants with chronic SCI were given a 6-month treatment of alendronate. The measurements taken in the study included BMD of the total body, upper extremity, lower extremity, and the trunk using DXA. After 6 months of treatment, there was no significant difference in BMD for the lower extremities between the treated and untreated groups.

Pharmacological treatments for the prevention of bone loss have more recently extended into the realm of targeting sclerostin. Sclerostin, being the Wnt inhibitor, ultimately prevents the formation of new bone. Sclerostin targeting antibodies have demonstrated positive effects in animal models when it comes to preventing significant bone loss following SCI (Beggs et al., 2015; Zhao et al., 2018). Both studies utilized rat models with complete spinal cord injuries that were administered Scl-Ab. In the study by Beggs et al. the rats experienced an increase in formation of bone and an increase in the osteoblast surface following three weeks of Scl-Ab administration immediately following SCI injury. In the study by Zhao et al., twelve weeks after SCI, the rats were given Scl-Ab for eight weeks. At the end of the eight weeks, the Scl-Ab improved the bone structure and promoted bone formation in the animals with SCI. Sclerostin inhibiting treatments are gaining traction as romosozumab became one of the first FDA approved medication to target sclerostin in people with osteoporosis (Graeff et al., 2015). Instead of strictly preventing bone resorption, the mechanism of bisphosphonates, romosozumab is a monoclonal antibody that binds and prevents sclerostin from inhibiting the Wnt signaling pathway. The drug has demonstrated

its ability to improve trabecular and cortical bone mass, structure, and stiffness in 3 months with continued effects 3 months post treatment. Given that there are potential secondary factors affecting SCI-induced osteoporosis, romosozumab is currently undergoing clinical trial testing on individuals with SCI based on the evidence in animal models (NCT04232657).

Aside from pharmacological treatments for osteoporosis and bone loss, regardless of the cause, physical rehabilitation techniques can also be used to promote bone formation. One treatment that has been studied is functional electrical stimulation (FES) cycling in individuals who have SCI (Frotzler et al., 2008; Lai et al., 2010; Mohr et al., 1997). In the early study by Mohr et al., ten individuals with chronic SCI took part in FES cycling for 12 months, three days a week, for 30 minutes a day, then six months of training once a week. The BMD at the proximal tibia after the 12 months of 3 days a week training had increased significantly. Following the reduced training, the BMD returned to its original value before training. Frotzler et al. also conducted a study on eleven individuals with chronic SCI who completed FES cycling for 12 months, several times a week for just under an hour on average. After 12 months, the trabecular and total BMD increased significantly at the distal femur. These studies demonstrate that there is the potential for FES cycling to play a role in improving the bone quality of individuals with chronic spinal cord injuries. In the more recent study by Lai et al., 24 individuals with acute SCI completed FES cycling exercises for three months, then stopped for three months (Lai et al., 2010). After three months of training, there was a decrease in the rate at which the individuals were losing BMD in the distal femur. Following three months without training, there was no longer a significant difference in BMD loss at the distal femur. These studies demonstrate that continuous FES cycling could reduce the bone loss in individuals with both acute and chronic SCI, but not necessarily prevent bone loss entirely.

Another potential non-pharmacological treatment for individuals with SCI includes the use of exoskeletons. There are many different types of exoskeleton devices that can be used on the upper or lower extremities. Although the different types and brands have varying configurations and overall structure, they all have the same basic functions. They use a combination of motors and servos to control the movement of the upper or lower extremities, allowing individuals with SCI to move and walk (Palermo et al., 2017).

This means that the Exoskeletons themselves can be used as a mobility aid, for those exoskeletons that are FDA approved for community use, like the Indego and the ReWalk (Mekki et al., 2018). They can provide those with SCI independence having the ability to move on their own. Exoskeletons that are not FDA approved for community use, but can be used in a medical facility with trained professionals, can play an important role in rehabilitation and therapy for individuals with SCI.

In addition to providing some independence for those with SCI, there is the potential for additional benefits associated with exoskeleton therapy including strengthening muscles and addressing secondary health concerns associated with SCI, such as spasticity, pain, and bone weakness (Mekki et al., 2018). It is also important to note that some studies assessing the effects of exoskeleton therapy list poor bone health as a contraindication for treatment (Palermo et al., 2017). This has the possibility to hinder the ability of studies to assess how exoskeleton therapy can affect bone health given that individuals having low quality bone might be at a risk for injury when using an exoskeleton. Despite this, one study in 2017 was conducted to evaluate how exoskeleton therapy impacted the overall BMD and body composition (Karelis et al., 2017). The study included five individuals with SCI and a mean time post injury of 7.6 years. Training was completed for six weeks three times a week for up to 60 minutes using the EKSO exoskeleton from EKSO bionics. In the end of the study, researchers concluded that there were significant increases in the cross-sectional area of individuals' calf muscles, but no statistically significant improvement in the individuals' tibial BMD. Another pilot study by Gordon et al. had twelve participants with SCI use a Lokomat, a supportive device that allows users to walk on a moving platform (Gordon et al., 2013). The participants complete six months of gait training, followed by six months without training, all while taking parathyroid hormone (PTH), calcium, and vitamin D supplements. At the conclusion of gait training, there were increases in BMD in the spine and hips, but it wasn't statistically significant. There was a statistically significant improvement in trabecular thickness in the distal femur. Although these findings support the potential for walking therapy to be enough to load the lower limbs to be therapeutically beneficial, there is a need for further research. Overall, there is a need for more studies to be conducting analyzing the effects of exoskeleton therapy on individuals' bone health.

Even though the exoskeletons provide the same basic function, the variation in the methods for controlling the exoskeletons, and the configuration of the components of the devices could have the potential to impact the effectiveness of the device when it comes to therapeutic benefits. Exoskeletons can vary in the number of actuating joints, having any combination of hip, knee, and ankle actuation. They can also range in their mechanisms for controlling the actuation, with many of them being trajectory controlled, meaning that the movement of the exoskeleton will always follow a set trajectory (Rodríguez-Fernández et al., 2021). This is especially crucial for those individuals who have complete loss of functionality in the lower extremities. The mechanism for initiating gait is also different for many exoskeletons. Some are initiated using a button or joystick, while others integrate sensors into the exoskeleton and sense shifts in weight, changes in center of pressure (COP), or other movement of the user (Rodríguez-Fernández et al., 2021). The possible variations in exoskeleton configurations indicates that there is a chance that there are differences in the movement and benefits associated with each exoskeleton. To the author's knowledge, there are no studies assessing the kinematics and kinetic differences between different types of exoskeletons.

Measurements of bone strength

The strength of bones is related to a number of properties of bones. It is well understood that bone is a viscoelastic anisotropic material, meaning that the amount of loading a bone can withstand is both dependent on the direction of loading, and the rate at which the loading occurs (Edwards et al., 2014; Hart et al., 2017). Bone itself is also a complex composite structure composed of a collagen matrix with hydroxyapatite dispersed throughout the matrix. The mechanical properties of bone can be best understood and interpreted by performing whole bone mechanical testing, which can be done in the form of a three-point, or four-point bending. This process can provide information regarding the overall strength, yield point, cyclic loading damage, effect of strain rate on strength, and how all of these factors relate to the overall microarchitecture of the particular bone being tested (de Bakker et al., 2017). Although this method of mechanical testing may be beneficial when it comes to understanding bone strength, it is a destructive

process that is only done ex vivo. To assess bone strength in vivo, non-invasive measurements and technology have been developed over the years. These methods vary in their capabilities and limitations, but overall provide researchers and clinician with similar information to that of physical bone mechanical testing.

One measure that is frequently used to assess bone strength is bone mineral density (BMD; g/cm^3). BMD is the measure of the amount of hydroxyapatite within a given volume. Hydroxyapatite, as aforementioned, is embedded in the collagenous matrix of the bone, and is the mineral form of calcium apatite. This mineral is partially responsible for the strength of bones. Having a higher density of bone mineral increases overall bone strength and can be an indicator for bone health as well. There are several methods for measuring BMD, one of the most common and simplest being dual x-ray absorptiometry (DXA) (Berger, 2002). DXA utilizes two different x-ray energies to penetrate the part of the body of interest. The higher the density and mineral content of the bone, the more energy the bone will absorb of the x-ray, and the less energy is measured on the other side of the body. This provides an estimate of bone density on a two-dimensional level that is referred to as areal BMD (aBMD; g/cm^2). Given that DXA computes the volumetric density of bone mineral using a two-dimensional imaging method, it is important to note that this cannot be a 'true' measure in changes in BMD (W. Brent Edwards & Schnitzer, 2015). A previous study has shown that DXA measurements have the potential to underestimate changes in BMD when compared to other imaging modalities, namely quantitative computed tomography (QCT) (Edwards et al., 2014).

In addition to DXA scans, an imaging technique that can also be used to assess bone health is QCT analysis. QCT analysis still uses x-rays, but is able to map out the bone being scanned in three-dimensions. The individual CT scans can be sliced across the imaging plane at a desired thickness to view a two-dimensional piece of the bone. Adding these slices on top of one another creates the full three-dimensional rendering of the bone being imaged. Individual three-dimensional pixels on the scans are known as voxels and can be smaller or greater depending on the resolution selected for the scan (Stagi et al., 2016). A higher resolution scan can also create more detailed images, allowing for better visualization of the

microarchitecture of the bone. By looking at the finer details of the bone structure, researchers can analyze the mechanism by which the bones change over time as a result of lack of loading, as is the case with SCI, or bone strength increases as a result of therapies (Kazakia et al., 2014). The CT scan can be calibrated to assess the density of the bone using calibration phantoms. These phantoms are regions in the scan that have a known hydroxyapatite density. The relationship between the Hounsfield units, or the units of measure given from the CT scan, can then be mapped to the density using these phantoms (Lang et al., 2006). This mapping, combined with the known locations and dimensions of the voxels, is combined to compute the overall BMD, or BMD at different regions of the bone.

And being able to assess bone density, QCT can be used to calculate other metrics of bone strength and geometry. Using the individual slices across the bone, the cross-sectional area (CSA; cm^2) of the bone at specific regions can be calculated. CSA is an important aspect of bone geometry that has a direct relationship on the bending strength of the bone. Having a higher CSA can impact the second moment of area for the bone, thus decreasing the bending stress in the bone for a given moment. A study by Siu et al. concluded that bone strength indices derived from cortical CSA (cortical BMD x cortical CSA) were better correlated to the load experienced at fracture than cortical BMD or overall BMD (Siu et al., 2003). Building off BMD, and general geometry measures, bone mineral content (BMC; g) can also be calculated using QCT data. Bone mineral content is the overall quantity of the bone mineral hydroxyapatite. Much like BMD, BMC can provide an indication of overall bone health and bone strength. BMC can be calculated by using the average density of the bone and multiplying it by the volume of the bone of interest, all of which can come from a QCT scan (Lang et al., 2006). BMC loss is a known effect of bone unloading and can thus contribute to weakened bones and increase fracture risk.

In addition to BMC there are other measures of bone strength, like compressive strength index, bending strength index, and bucking ratio. The compressive strength index (CSI; g^2/cm^4) can be based off of BMD and CSA. As defined by Edwards et al. the equation for CSI is $iBMD^2*CSA$, where iBMD is the integral bone mineral density of volumetric bone density (Edwards et al., 2014; Lang et al., 2004). Integral, in this case, meaning all voxels within the periosteal surface of the bone. In this study, CSI was shown to have a

high correlation to compressive stiffness as predicted by finite element modeling, indicating that CSI may provide important information regarding the mechanical properties of bone. Similar to CSI, bending strength index (BSI; cm^3) can also provide researchers information regarding how bone will behave in response to loading. BSI, as described by Cheng et al. is dependent on the elastic modulus weighted moments of inertia of the bone's cross section, and the width of the bone (Cheng et al., 2007; T. Lang et al., 2004). The elastic modulus weighted moments of inertia are calculated using the BMD of each voxel in the cross-section of the bone (Cheng et al., 2007; T. Lang et al., 2004). Buckling ratio (BR) is another measure of bone strength that has demonstrated some predictability for assessing the likelihood of a fracture in bone as well in the case of femoral necks. BR is determined by the ratio of the cortical thickness index to the effective bone half-width. The cortical thickness index is based on the total volume of the femoral neck, the length of the femoral neck, and the volume of the cortical bone in the region of interest (ROI). The effective bone half width, on the other hand, is calculated using the femoral neck length and volume (Cheng et al., 2007).

Table 1: Common measurements of bone geometry and strength

Measurement	**Description**	**Equation**
Cross-sectional area CSA (cm^3)	Area of individual slices of bone in specific regions average over total region of interest	$CSA = \frac{\sum_i^{n_{slices}} n_{voxels,i} * area_{voxel}}{n_{slices}}$
Bone volume BV (cm^3)	Number of voxels multiplied by the volume of each voxel	$BV = n_{voxels} * vol_{voxels}$
Bone mineral content BMC (g)	Average of the voxel density multiplied by the bone volume	$BMC = \frac{\sum_i^{n_{voxels}} \rho_{voxels,i}}{n_{voxels}} * BV$
Bone mineral density BMD (g/cm^3)	Average density throughout the bone	$BMD = BMC/BV$
Compressive strength index CSI (g^2/cm^4)	Index based on average bone mineral density and	$CSI = BMD^2 * CSA$

	average cross-sectional area of region of interest (Lang et al., 2006)	
Bending strength index BSI (cm^3)	Is the sum of the effective moments of inertia divided by the diameter of a circular cross-section equivalent area (Lang et al., 2004)	$$BSI = \frac{I_X + I_Y}{W}$$ $$I_X = \frac{1}{e_b}\sum_i e_i * (x_i - \bar{x})^2 * area_{voxels}$$ $$I_Y = \frac{1}{e_b}\sum_i e_i * (y_i - \bar{y})^2 * area_{voxels}$$ $$W = 2 * \sqrt{\frac{CSA}{\pi}}$$
Cortical thickness index iCThi (cm)	Related to the ratio of cortical tissue volume to total bone tissue in the ROI	$$iCThi = 0.5 * \left[\sqrt{\frac{iBV_{reg}}{length_{reg}}} - \sqrt{\frac{iBV_{reg} - cBV_{reg}}{length_{reg}}}\right]$$
Buckling ratio BR	The ratio of the cortical thickness index to the effective bone half width(Cheng et al., 2007)	$$BR = iCThi/iBTHi$$ $$iCThi = 0.5 * \left[\sqrt{\frac{iBV_{reg}}{length_{reg}}} - \sqrt{\frac{iBV_{reg} - cBV_{reg}}{length_{reg}}}\right]$$ $$iBThi = 0.5 * \sqrt{\frac{iBV_{reg}}{length_{reg}}}$$

n_{slices} : number of slices in ROI
n_{voxels} : number of voxels in ROI
$area_{voxel}$: area of each voxel in the transverse plane
vol_{voxels} : volume of each voxel
ρ_{voxels} : density of each voxel
e_b : cortical bone elastic modulus
e_i : equivalent elastic modulus of each voxel
x_i, y_i : coordinates of the i^{th} voxel
$\bar{x}, \bar{y}$: elastic modulus weighted centroid
W : diameter of a circular cross-section equivalent area
I_x, I_y : effective polar moments of intertia
iBV_{reg} : integral bone volume of region of interest
$length_{reg}$: length of region of interest
cBV_{reg} : cortical bone volume of region of interest

Summary

Bone remodeling is an important mechanism by which bone is broken down and rebuilt by osteoclasts and osteoblasts. This process of remodeling is a carefully coupled system that is regulated by a series of responses as a result to stimuli. One of the crucial stimuli for the maintenance of bone's integrity is mechanical loading. Although the specific mechanisms by which bone cells sense mechanical loading are not fully understood, the necessity of loading is widely accepted. When mechanical loading is removed from bone altogether, as is sometimes the case in individuals with SCI, the bone remodeling mechanism is no longer balanced. More bone is resorbed than is being formed, leading to SCI induced osteoporosis. SCI-induced osteoporosis is known to cause weakened bone and severe bone loss, causing bones to be extremely susceptible to fractures that can lead to secondary health conditions. In order to image and assess the progression of SCI-induced osteoporosis, there are different technologies to measure the bone strength, geometry and quality, notably DXA scans and QCT analysis. They both have the ability to calculate a measure of bone density, aBMD for DXA and BMD for QCT analysis, and BMC, important metrics associated with bone quality, but QCT provides a three-dimensional rendering of the bone being imaged. There are well-established methods to assess bone strength and geometry using both of these methods as well. Despite SCI-induced osteoporosis being a common problem among those with SCI, treatments for SCI-induced osteoporosis are limited to bisphosphonates, and more recently anti-sclerostin antibodies undergoing clinical trial testing. An alternative to pharmacological treatments would be the use of physical rehabilitation and therapy, that could use FES cycling, or the use of exoskeletons. FES cycling has demonstrated some promise at slowing bone loss in individuals with SCI but may not be enough to prevent bone loss altogether. Exoskeleton walking therapy has the potential to be able to load the affected extremities enough to have therapeutic effects, but the numbers of trials and studies assessing this are limited. Given this gap in current research, the aim of this study was to determine whether or not exoskeleton walking therapy had an effect on bone quality in individuals with SCI.

This thesis uses data that are part of a greater clinical trial including individuals with chronic SCI. The clinical trial is an ongoing crossover study with 6 months of exoskeleton walking therapy. The purpose of the following chapters is to assess the effects and characteristics of exoskeleton walking therapy in individuals with SCI using QCT, video data, and pressure sensing insole data. The following chapters will be submitted as individual manuscripts, and each chapter addresses one aim for this thesis. In Chapter 3, we quantified the changes in tibia and femur bone volume and bone mineral content before and after exoskeleton therapy. In Chapter 4, we calculated net knee joint contact force and moment based on kinematics of exoskeleton therapy videos and pressure sensing insole data. In Chapter 5, we determined the relationship between candidate measures of "loading dose" and exoskeleton-driven bone mineral content changes.

Chapter 3: Calculating changes in integral bone mineral content of regions of the distal femur and proximal tibia following exoskeleton walking therapy

Introduction

It is a well-established fact that bone remodeling is impacted by the loading in which it experiences (Battaglino et al., 2012; Garland et al., 2001, 2008; Lobos et al., 2018; Leslie R. Morse et al., 2019; Zehnder, Lüthi, et al., 2004). Bone remodeling is a carefully coupled system of breaking down and rebuilding bone in response to loading and strains experienced by osteoclasts within the bones (Robling & Bonewald, 2020). When loading is removed from bones altogether, there can be a substantial loss in bone as the coupled system becomes destabilized. This bone loss is especially prevalent in individuals who have sustained an SCI. With an SCI that results in loss of lower limb function, there is a drastic reduction in the loading experienced by the lower limbs. Reducing the forces applied to the lower extremities causes the rapid loss of bone and the deterioration of bone strength altogether (Garland et al., 2001, 2008; Lobos et al., 2018; Leslie R. Morse et al., 2019). Preserving bone quality and strength is crucial in preventing fractures that can lead to secondary health problems. To better understand the loss of bone, and the effects of therapy on bone quality, there are different types of technology and methods to measure bone strength and geometry. Well-established methods use QCT to create three-dimensional models of the bone (Cheng et al., 2007; Edwards et al., 2014; Lang et al., 1997). Specifically, these methods allow for the assessment of total integral BMC (iBMC) within a bone. In iBMC, the total BMC within the periosteal surface is calculated. iBMC can be an indicator for overall bone strength and determine whether a therapeutic intervention has improved bone quality.

In recent years, exoskeleton walking therapy has demonstrated its potential to be used as a therapeutic intervention for those with SCI(Gordon et al., 2013; Karelis et al., 2017). Despite this, longitudinal studies analyzing the effects of walking therapy on BMC with substantial sample sizes are lacking. Here, our purpose was to utilize QCT analysis to determine if there are any changes in iBMC of the distal femur and proximal tibia in individuals with SCI undergoing walking therapy.

Methods

Participants

Individuals with spinal cord injury were recruited as part of a larger ongoing clinical trial, the purpose of which is to evaluate skeletal benefits from regular exoskeleton assisted walking therapy (NCT02533713). To enroll in the trial, individuals have to be AIS-A or AIS-B, 3-10 years post-injury, free of known cardiovascular disease, and 40 years or younger. Additionally, participants must have complete thoracic SCI (T3-T12), be between 158-188 cm in height, weight under 100kg, and have a Modified Ashworth Scale (MAS) score of less than 3 in both legs, and have enough strength in the upper body to complete sit to sit transfers. The present study included 13 participants (12 male and 1 female, age: 36.2 ± 8.6 years, height: 179.0 ± 8.0 cm, mass: 79.1 ± 13.08 kg). All participants gave written informed consent to participate in this institutionally approved research study.

As part of the clinical trial, each participant was assigned to walking therapy in an exoskeleton for three hours per week, for six months. All walking therapy was supervised by trained physical therapists and occurred within the PEAK Center at Craig Rehabilitation Hospital (Englewood, CO). The majority of the therapy sessions were performed using an Indego exoskeleton (Indego; Parker Hannifin, Cleveland, OH); however, some participants also used an Ekso exoskeleton (ekso Bionics, Richmond, CA) for some sessions.

CT Scans

CT scans were taken of both legs for each participant (Revolution CT, GE Medical Systems; pixel resolution 0.352 mm, slice thickness 1.25 mm, 100 mA*s, 120 kVp, 30 cm scan length for 15 cm each of distal femur and proximal tibia) at zero (baseline scans), 6 (second), and 12 (third) months after the trial began. In each scan, a calibration phantom with known hydroxyapatite concentration was placed in between the legs of each participant (custom made calibration phantom standards for 0, 400, and 800 mg HA/cm^3) (Figure 1). The phantoms were used to convert the CT Hounsfield units to bone density for each scan.

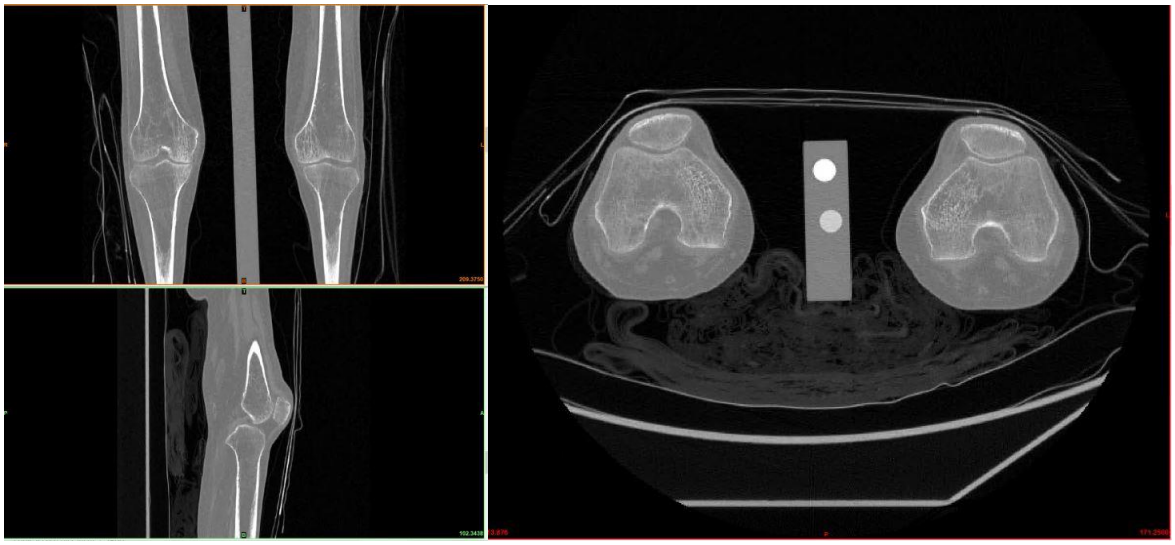

Figure 1: CT Scans of both legs with calibration phantom

CT Alignment

The distal femur and proximal tibia were analyzed and aligned separately. Baseline CT images were manually aligned along the longitudinal axes of the femur and the tibia using Mimics (Materialise, Leuven, Belgium). Second and third scans were registered using a proven registration method demonstrated by Edwards et a. with a combination of Mimics and Matlab software (MathWorks, Natick, MA, USA) (W. B. Edwards et al., 2013, 2014). The epiphysis, metaphysis, and diaphysis were marked as 10, 20, and 30% of the total length of the bone from the distal femur and proximal tibia. Femur and tibia lengths were calculated using participant heights and anthropometric calculations from Winter (Edwards et al., 2013).

QCT Mineral Analysis

The relationship between equivalent bone density (ρ_{HA}) and Hounsfield units was established using a linear equation developed using the calibration phantom: $\rho_{HA} = (1.2\pm0.01)*HU + (24.8\pm4.5)$. The periosteal surface was identified using a density threshold of 0.15g/cm^3 (Figure 2). In regions where the cortical shell was thin due to the bones having a lower density, primarily at the epiphysis and metaphysis, manual identification of the periosteal surface was performed (Figure 3). Integral, cortical, and trabecular regions were identified using methods similar to Edwards et al. (Edwards et al., 2014). Integral regions were comprised of all voxels within the periosteal surface. Trabecular regions were identified using a

3.5mm in plane erosion from the integral region. The cortical region was selected using a Boolean operation subtracting the trabecular region from the integral region. A threshold of 350 mg/cm^3 was applied to the cortical region to obtain only the voxels that fall within the density range for cortical bone. The integral bone volume (cm^3) was calculated as the total volume within the periosteal surface by multiplying the number of voxels by their known size using Matlab 2019 (Simulink, Natick, MA). We also calculated total femoral and tibial iBMC by averaging the density of each voxel and multiplying by the integral bone volume, and the iBMC at the epiphysis, metaphysis, and diaphysis.

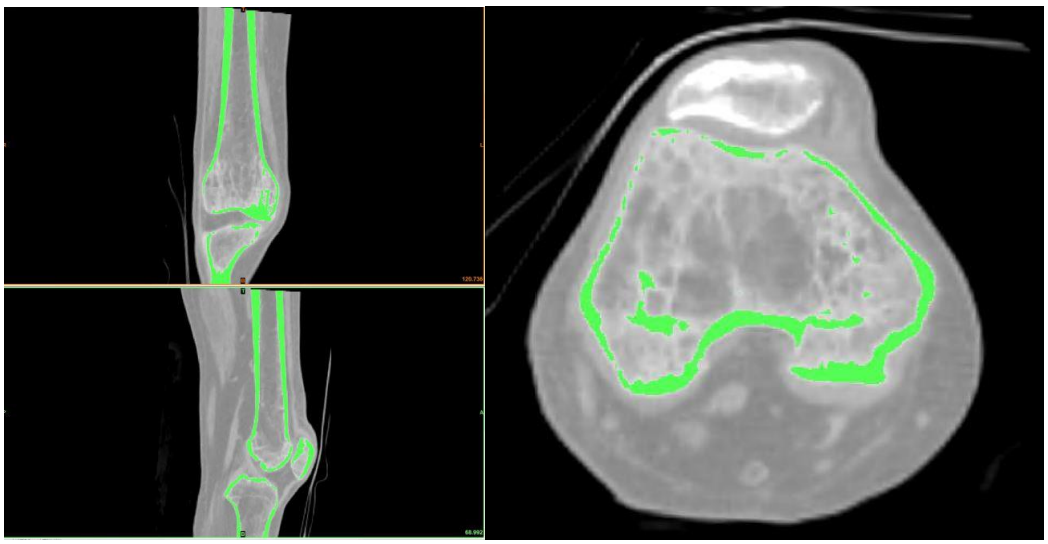

Figure 2: CT scans with thresholding without manual identification of periosteal surface

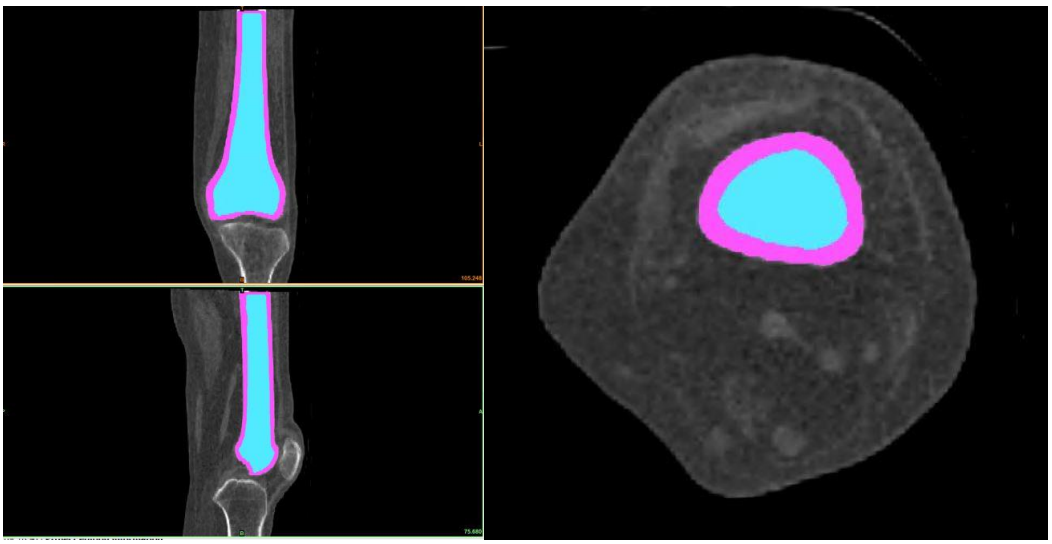

Figure 3: CT scans with manual identification of periosteal surface with cortical region (pink) and trabecular region (blue)

Statistical Analysis:

Statistical analyses were performed using SPSS v. 23 (IBM, Armonk, NY). To test our hypothesis that exoskeleton walking therapy can increase iBMC, we used repeated measures ANOVA compare the individual measures of iBMC before and after walking therapy in both left and right legs. For those variables with significant time-related effects, post hoc paired t-tests with Bonferroni corrections were used to make individual comparisons.

Results

In this study, we analyzed data from ten left femurs and tibias, and 13 right femurs and tibias from 13 participants. The average iBMC at the epiphyseal region in the femur and tibia and the total iBMC in the femur increased after walking therapy ($p \leq 0.023$ and $p=0.038$; Table 2). Average iBMC of the femur and tibia in the epiphyseal region increased by 8.34 ± 11.60 % and 4.23 ± 9.80 %. The average change in the total iBMC of the femur was 2.40 ± 4.83%.

Table 2: Paired sample statistics and multivariate test significance

Multivariate significance		Mean (g)	Average change in iBMC (g)	p-value
Femur (p = 0.000)	FDia_iBMC1	14.311 (2.84)	-0.08 (0.29)	0.199
	FDia_iBMC2	14.230 (2.87)		
	FMet_iBMC1	12.109 (3.69)	-0.07 (0.48)	0.498
	FMet_iBMC2	12.041 (3.49)		
	FEpi_iBMC1	13.869 (4.54)	+0.91 (1.21)	**0.002**
	FEpi_iBMC2	14.776 (4.31)		
	FTot_iBMC1	40.289 (10.42)	+0.76 (1.64)	**0.038**
	FTot_iBMC2	41.046 (10.01)		
Tibia (p = 0.038)	TEpi_iBMC1	10.110 (3.87)	+0.48 (0.94)	**0.023**
	TEpi_iBMC2	10.590 (4.25)		
	TMet_iBMC1	12.115 (3.22)	-0.05 (0.67)	0.723
	TMet_iBMC2	12.065 (3.16)		
	TDia_iBMC1	15.339 (3.77)	-0.26 (0.98)	0.206
	TDia_iBMC2	15.074 (3.47)		

	TTot_iBMC1	37.564 (10.04)	+0.16 (2.16)	0.720
	TTot_iBMC2	37.728 (10.13)		

FEpi_iBMC1, FMet_iBMC1, FDia_iBMC1 : femoral iBMC at the epiphyses, metaphyses, and diaphysis for time point 1, before walking therapy
FEpi_iBMC2, FMet_iBMC2, FDia_iBMC2 : femoral iBMC at the epiphyses, metaphyses, and diaphysis for time point 2, after walking therapy
FTot_iBMC1 : total femoral iBMC for time point 1, before walking therapy
FTot_iBMC2 : total femoral iBMC for time point 2, after walking therapy
TEpi_iBMC1, TMet_iBMC1, TDia_iBMC1 : tibial iBMC at the epiphyses, metaphyses, and diaphysis for time point 1, before walking therapy
TEpi_iBMC2, TMet_iBMC2, TDia_iBMC2 : tibial iBMC at the epiphyses, metaphyses, and diaphysis for time point 2, after walking therapy
TTot_iBMC1 : total tibial iBMC for time point 1, before walking therapy
TTot_iBMC2 : total tibial iBMC for time point 2, after walking therapy

Discussion

The effects of exoskeleton walking therapy on bone remodeling is still an ongoing area of research. The question we aimed to answer with this study was whether or not walking therapy increased the amount of bone within an individual's tibia and femur. The purpose of this study was to characterize the changes in iBMC in different regions of the tibia and femur, and the total iBMC of both bones. We achieved this by using a combination of QCT analysis with Mimics software and mineral calculations using Matlab of the CT scans before and after walking therapy. We determined that there was a significant increase in iBMC at the epiphyseal region of the femur (8.34 ± 11.60 %) and tibia (4.23 ± 9.80 %) and the total femur iBMC (2.40 ± 4.83%) before and after walking therapy ($p \leq 0.023$ and $p=0.038$; Table 2).

During the acute stages of SCI, there is a drastic reduction in iBMC, namely in the proximal tibia and distal femur. These decreases were most drastic in the epiphyseal regions of the proximal tibia and distal femur, reaching up to 3-3.6% iBMC loss per month (Biering-Sorensen & Schaadt, 1990; Edwards et al., 2015; Eser et al., 2004; Jiang et al., 2006; Szollar et al., 1997). The individuals in this study were 3-10 years post injury, meaning that they were in the chronic stage of SCI. It has been debated whether or not bone loss reaches a steady-state after 2 years, 3-8 years, or as long as 19 years after injury (Battaglino et al., 2012). Other research has found that there may be a positive correlation between bone loss and time

since injury in trabecular rich regions (Edwards et al., 2015; Eser et al., 2004). The bone loss that occurs following an SCI has been described using an exponential decay curve (Edwards et al., 2015; Eser et al., 2004). Based on the understanding that bone loss reaches a steady-state after 2 years, or 3-8 years, the individuals in this study should have reached, or are almost at a steady-state of bone loss. The iBMC loss at the metaphyseal and diaphyseal regions of the tibia and femur, and the total iBMC loss in the tibia, was not significant, which could be a result of the bone loss reaching an equilibrium. Given that this was a crossover study, the observational time period can provide information about if the bone loss had reached that steady-state.

The significant change in iBMC indicates that exoskeleton walking therapy may have an impact on bone remodeling. Other variables demonstrated non-significant decreases, thus the individual were at their steady-state of bone loss. Provided that the only significant changes to the variables were positive, exoskeleton walking therapy appears to disrupt this bone loss and induce bone formation. The epiphyseal region, being trabecular rich, has demonstrated the highest decrease in BMC in prior longitudinal studies assessing loss in BMC following SCI (National Spinal Cord Injury Statistical Center, 2018). Given that this is one of the few regions to have significant changes in the iBMC before and after walking therapy, this could provide some indication of how the bone is responding to the walking therapy.

There were several limitations associated with this study. One limitation was the relatively small sample size. The CT scans are part of an ongoing clinical trial and post walking therapy data for some individuals are still in the process of being collected. In some instances, there were missing scans, or missing individual sides for those who were unable to return for post-walking therapy scans, or who missed one side during the scan. Additionally, some individuals did not complete the clinical trial.

In summary, we calculated and compared the iBMC of regions in the distal femur and proximal tibia following exoskeleton walking therapy in individuals with chronic SCI. We observed significant increases in the epiphyseal iBMC in the femur and the total iBMC for the femur. The epiphyseal iBMC in the tibia also increased, but not significantly. All other measures of iBMC experienced a slight decrease

following walking therapy, but none of these changes were significant. The results of this study demonstrate that walking therapy has the potential to induce changes in the iBMC in specific regions in the lower limbs.

Chapter 4: Kinematics and kinetics of exoskeleton-assisted walking in people with spinal cord injury: Comparison of two different exoskeletons

Introduction

Approximately 294,000 people are living in the United States with a spinal cord injury (SCI) (National Spinal Cord Injury Statistical Center, 2018). Spinal cord injuries can impact the quality of people's lives by limiting mobility in the lower extremities and creating high cost health problems over time. The average yearly health costs and medical expenses for people with spinal cord injuries can range from $45,000 to $1,000,000 (National Spinal Cord Injury Statistical Center, 2018). This can increase with subsequent re-hospitalizations, which occur in about 30% of people with SCI (Carbone et al., 2013b; Dejong et al., 2013). A fracture in a person with SCI is likely to cause a number of problems associated with re-hospitalization, including urinary tract infections, pneumonia, and pressure ulcers (Bauman & Cardozo, 2015; Chantraine et al., 1986; Jiang et al., 2006).

People with SCI are at a high risk of fracture due to the bone loss that occurs as a result of their injuries (C. H. Turner, 1998). Bone adapts to its mechanical loading environment. In individuals with SCI, the lack of mobilization and weight-bearing in the lower extremities are major contributors to bone loss (Battaglino et al., 2012). There are limited options for therapies in individuals with spinal cord injuries. Some include drugs to treat osteoporosis (for example, bisphosphonates and antisclerostin antibodies, mechanical and electrical stimulation of the lower extremities, and mechanical stimulation using vibrations (Baunsgaard et al., 2018).

Recently, exoskeletons have become more widely available to the rehabilitation community. These represent a potentially unique method of mechanical loading on lower limbs for people with SCI. Exoskeleton devices have been used in therapy for individuals with SCI to improve gait function and balance by inducing movement in the lower limbs using motors (C. H. Turner, 1998). Exoskeleton walking therapy applies moments and forces at ankle, knee, and hip joints to allow a person to walk with assistance, and bear weight through the lower extremities (Talaty et al., 2013). Being able to calculate the moments

and forces within the ankles and knees during exoskeleton therapy can provide information about how much the joints are loaded (Cheu et al., 2018). We currently do not know whether exoskeleton walking therapy can adequately load the lower limbs to provide therapeutic benefits to the bone of individuals using them. Furthermore, forces occurring within the user's ankles and knees may differ depending on the type of exoskeleton. Additionally, the use of mobility aids, such as walkers and crutches, may decrease the forces transmitted through the ankles and knees, decreasing the likelihood of benefits to bone.

Here our purpose was to utilize video motion capture and pressure sensing shoe insoles to determine the kinematics and kinetics at the ankles and knees of individuals with SCI during exoskeleton walking therapy. Secondarily, we compared gait kinematics and kinetics during walking between two different types of exoskeletons. Characterizing exoskeleton walking dynamics is important to determine potential benefits of these devices and for establishing safety criteria to prevent injury in users.

Methods

Participants

Individuals with spinal cord injury were recruited as part of a larger ongoing clinical trial, the purpose of which is to evaluate skeletal benefits from regular exoskeleton assisted walking therapy (NCT02533713). To enroll in the trial, individuals have to be AIS-A or AIS-B, 3-10 years post-injury, free of known cardiovascular disease, and 40 years or younger. Additionally, participants must have complete thoracic SCI (T3-T12), be between 158-188 cm in height, weight under 100kg, and have a Modified Ashworth Scale (MAS) score of less than 3 in both legs, and have enough strength in the upper body to complete sit to sit transfers. The present study had an additional limitation of shoe size (due to our pressure-sensing insoles) and included 12 participants (11 male, 1 female age: 36.3 ± 9.0 years, height: 177.8 ± 7.6 cm, mass: 77.4 ± 12.8 kg); Table 3). All participants gave written informed consent to participate in this institutionally approved research study.

Table 3: Participant Demographic Information

Participant ID	Age	Sex	Height (cm)	Baseline Weight (kg)	Exoskeleton(s)
1010	48	Male	175.26	82.628	Indego
1011	39	Male	182.88	78.996	Ekso
1013	23	Male	172.72	82.174	Indego
1018*	24	Male	185.42	84.898	Both
1023	28	Male	177.8	69.235	Indego
1028*	50	Male	172.72	105.782	Indego
1040	38	Male	190.5	53.4358	Ekso
1041	43	Male	182.88	78.996	Both
1055**	27	Male	180.34	67.873	Both
1059	35	Female	162.56	70.824	Indego
1064$**	40	Male	180.34	84.898	Indego
1070	40	Male	170.18	69.235	Indego

* = missing video data

** = missing pressure data using the EKSO

$ = foot cut off in video data

As part of the clinical trial, each participant was assigned to walking therapy in an exoskeleton for 3 hours per week, for 6 months. All walking therapy was supervised by trained physical therapists and occurred within the PEAK Center at Craig Rehabilitation Hospital (Englewood, CO). The majority of the therapy sessions were performed using an Indego exoskeleton (Indego; Parker Hannifin, Cleveland, OH); however, some participants also used an Ekso exoskeleton (ekso Bionics, Richmond, CA) for some sessions. During the last month of the 6-month intervention, video recordings and pressure-sensing insole data were collected during one of the therapy sessions. Three participants returned to the clinic one month later for video and pressure-sensing insole data collection on the other exoskeleton.

Video and Force Data Collection

During the data collection session, sagittal plane videos were recorded of each participant walking in a straight line in front of a plain wall. A meter stick was placed on the wall to provide a scale within each video image. White circular stickers were placed on the lateral toe, ankle, knee, and hip of the exoskeleton. The toe marker was placed directly on the participant's shoe for the Indego, and on the lateral foot plate for the EKSO. The position of each participant's heel was estimated manually, based on the toe position while the foot was flat on the floor. Using these markers, we tracked the sagittal plane movements of the thigh, shank, and foot that were facing the camera throughout the gait cycle.

Simultaneously, pressure sensing insoles (Orpyx LogR, Orpyx, Calgary, Alberta, Canada), were used to capture data regarding the center of pressure (COP) location and foot plantar surface reaction force (PRF) magnitude for each foot. In a small validation study using able-bodied individuals, we found that PRF during walking visually matched forceplate data (Id et al., 2019). The data capture was synchronized with the video footage using a timer, with temporal alignment visually confirmed at heelstrike by the investigators who performed the analysis (NM and KLT). Key outcomes included peak PRF and time of peak (expressed as percent stance), peak PRF loading rate (calculated as the maximum slope of the PRF versus time curve), cadence, stance time, and swing time (expressed as a percent of the total gait cycle).

Kinematics Calculations

To track the position of the markers during the gait cycle, we used the free motion analysis software Kinovea (Y. Fang et al., 2017). First, the video was scaled using the meter stick. Next, a point was placed at the position of each marker and tracked throughout the course of the motion. Within the global coordinate system of the video image, the x and y-coordinates of each point with reference to its starting position were then exported to a spreadsheet. We assumed that the participant kinematics were identical to the exoskeleton kinematics in the sagittal plane. The kinematic analysis included the entire gait cycle and a single gait cycle was measured for each video recording. An average of 2.2 ± 0.7 videos were measured for each participant.

We defined the knee angle as the angle between the shank and the thigh on the posterior side of the participant, and the ankle angle as the angle between the foot and the shank on the anterior side of the participant (Figure 4). Key outcomes included knee and ankle angles over the entire gait cycle, and range of motion (maximum – minimum) during the gait cycle. Average walking speed and stride length were collected from the outputs given by the exoskeleton if available. If unavailable, the stride length and walking speed were calculated using the distance the foot traveled, and the distance over time respectively based on the video footage.

Figure 4: Orientation of knee and ankle angles during walking therapy

Kinetic Calculations

To calculate the net joint forces and moments at the ankles and knees, we calculated segment centers of mass (COMs) and moments of inertia using SCI specific anthropometric data (Id et al., 2019). The kinetic analysis was limited to the stance phase, defined as heel-strike to toe-off. Because the pressure-sensing insole measured the force at the plantar surface of the foot, the net joint forces and moments calculated here reflect those experienced by the user and do not include inertias or masses of the exoskeleton itself. A recursive Newton-Euler approach was used, neglecting the mass of the shoes (Equations 1-4).

$$\overline{F_{ank}} + \overline{PRF} + m_{foot}\bar{g} = m_{foot}\overline{a_{foot}} \quad (1)$$

$$\overline{\tau_{ank}} + \overline{r_{ank}} \times \overline{F_{ank}} + \overline{r_{PRF}} \times \overline{PRF} = I_{foot}\alpha_{foot} \quad (2)$$

$$\overline{F_{knee}} - \overline{F_{ank}} + m_{shank}\bar{g} = m_{shank}\overline{a_{shank}} \quad (3)$$

$$\overline{-\tau_{ank}} + \overline{\tau_{knee}} + \overline{r_{knee}} \times \overline{F_{knee}} + \overline{r_{ank}} \times -\overline{F_{ank}} = I_{shank}\alpha_{shank} \quad (4)$$

Here, $\overline{F_{ank}}$ is the net force across the ankle, $\overline{PRF}$ is the plantar surface reaction force as explained previously, m_{foot} is the mass of the foot, $\bar{g}$ is the acceleration due to gravity, and $\overline{a_{foot}}$ is the linear acceleration of the entire foot determined from the video data (Rodríguez-Fernández et al., 2021). $\overline{\tau_{ank}}$ is the net ankle joint moment, $\overline{r_{ank}}$ is the vector from the COM of the foot to the ankle marker and $\overline{r_{PRF}}$ is the vector from the COM of the foot to the location of the PRF (the center of pressure). We assumed that the PRF acted perpendicular to the bottom of the foot. I_{foot} is the moment of inertia of the foot about its COM and α_{foot} is the angular acceleration of the foot, determined from the video data. Key outcomes included net joint forces and moments at the ankle and knee during the stance phase, and peak ankle and knee moments.

Statistical Analysis

Means of all outcome variables were calculated across all gait cycles for each participant in each type of exoskeleton. Descriptive statistics were calculated for each of the outcome variables, and were assessed for normality. To account for differences in body size, forces were normalized by body mass and moments were normalized by body mass*height. Related variables (for example, all temporal/spatial variables) were grouped together in multivariate analysis of variance (ANOVA) to compare the two types of exoskeletons. Although 3 of our 12 participants walked in both exoskeletons, data from the two exoskeletons were treated as independent and we did not consider participant to be a repeated measure. For all variables we examined the univariate contributions using independent sample t-tests. All calculations were performed using SPSS v. 23 (IBM, Armonk, NY) and we considered α=0.05 to be significant.

Results

Knee and ankle kinematics were significantly different between the two types of exoskeletons. The knee and ankle ranges of motion and maximum angles (Figure 5) were significantly higher in the Indego than the EKSO (Table 4). Participants using the EKSO had significantly slower stride times than those using the Indego (Table 4).

Although the net joint forces and peak PRF did not reach one body weight for the EKSO and exceeded one body weight for the Indego, the differences were not significant due to the small sample size and large between-participation variation (Figure 6). Similarly, most net joint moments were not significantly different between devices, although the means were about twice as large in the Indego versus the EKSO (Figure 7). Only the maximum ankle moment was different between the two exoskeletons, with the EKSO moment being 64% smaller than that of the Indego (Table 4; $p \leq 0.043$).

Multivariate tests confirmed significant differences in kinematics and temporal variables between the two exoskeletons. All kinematic variables except for minimum knee angle were significantly different, with the Indego achieving a 73% and 35% larger range of motion at the ankle and knee, respectively. In the temporal multivariate test, stride time and ten-meter walking speed were both significantly different between exoskeletons. Walking in the Indego is 50% faster, resulting in a 31% shorter stride time.

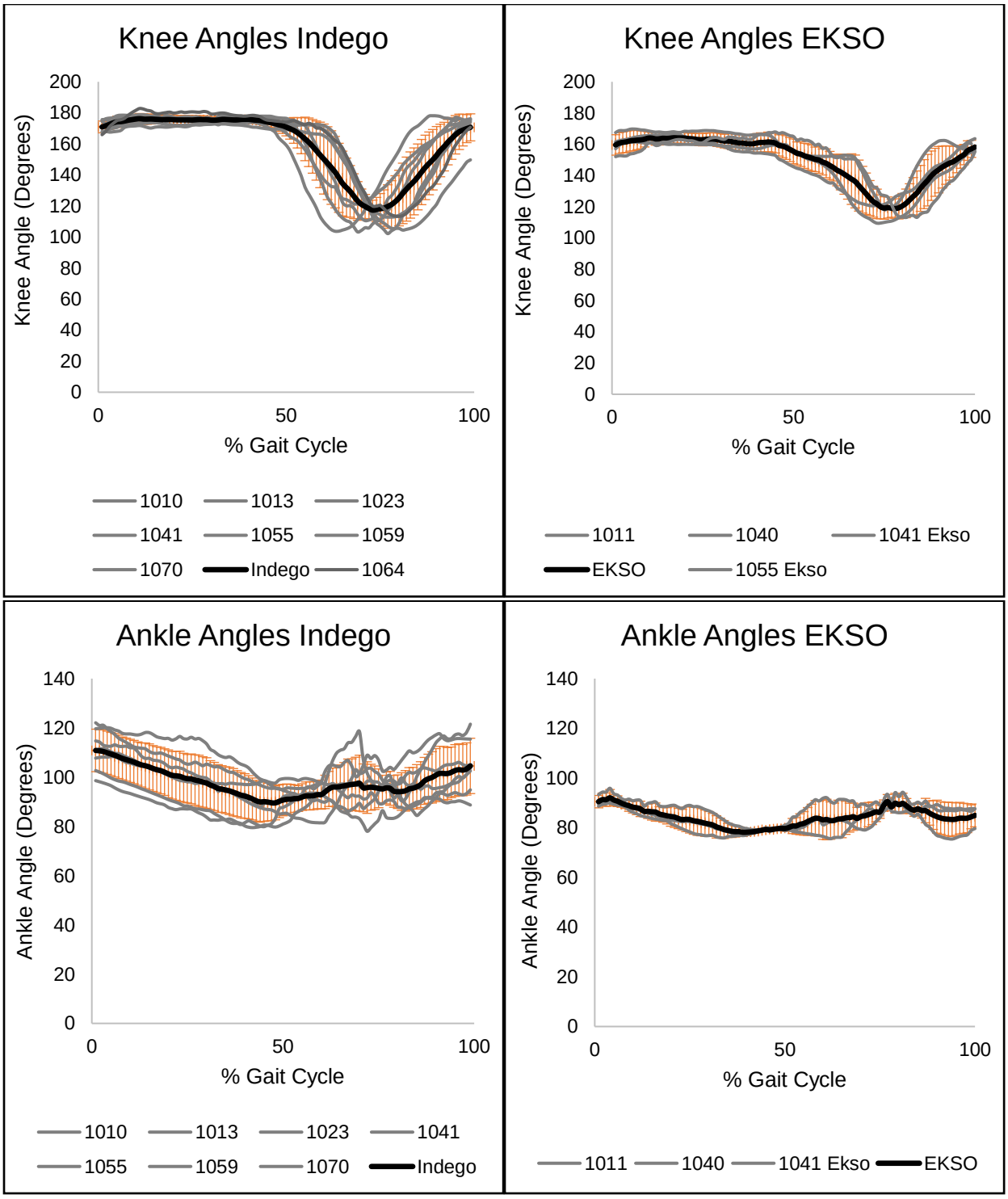

Figure 5: Knee and ankle kinematics versus gait cycle for both exoskeletons

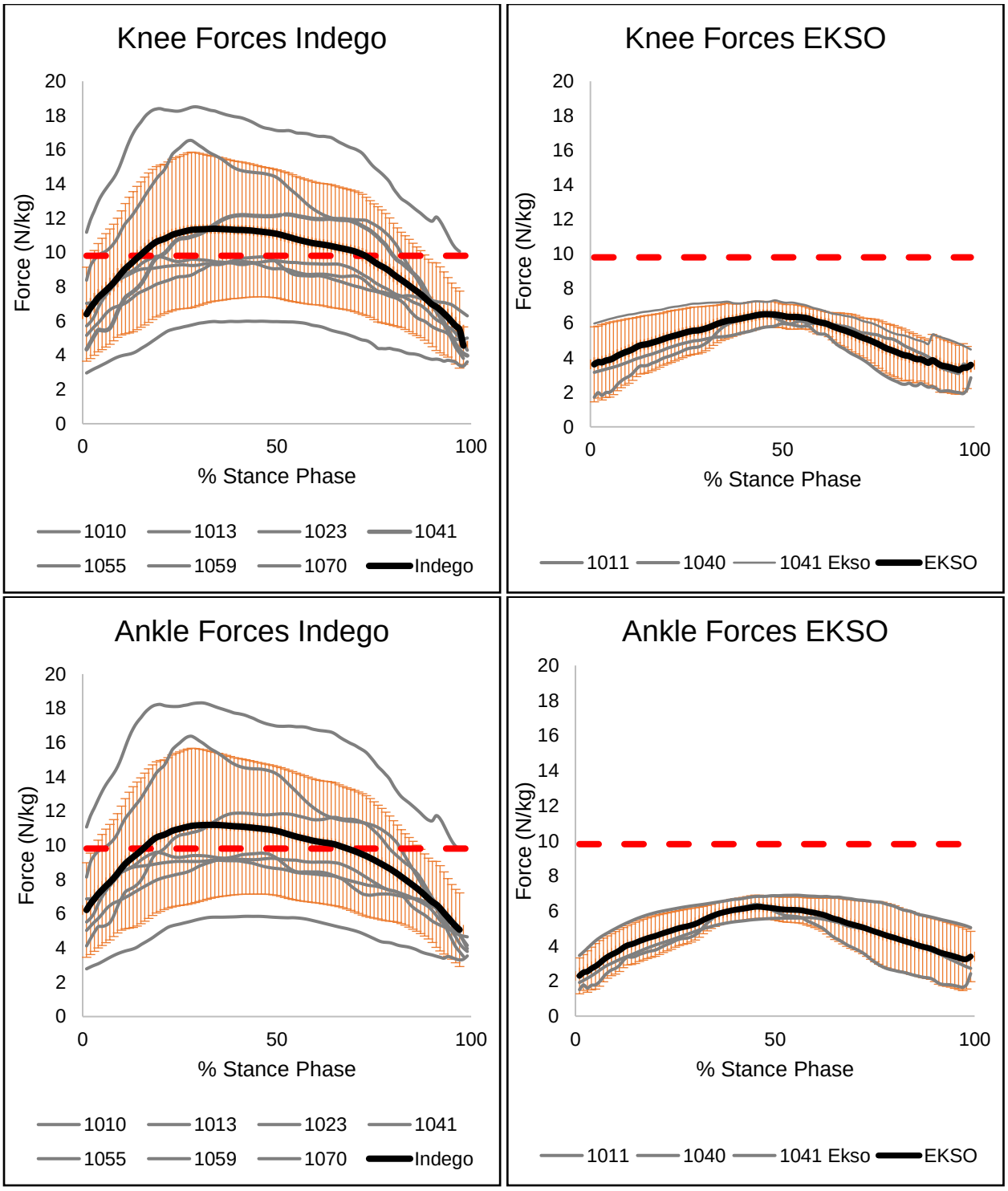

Figure 6: Knee and ankle forces versus stance phase for both exoskeletons

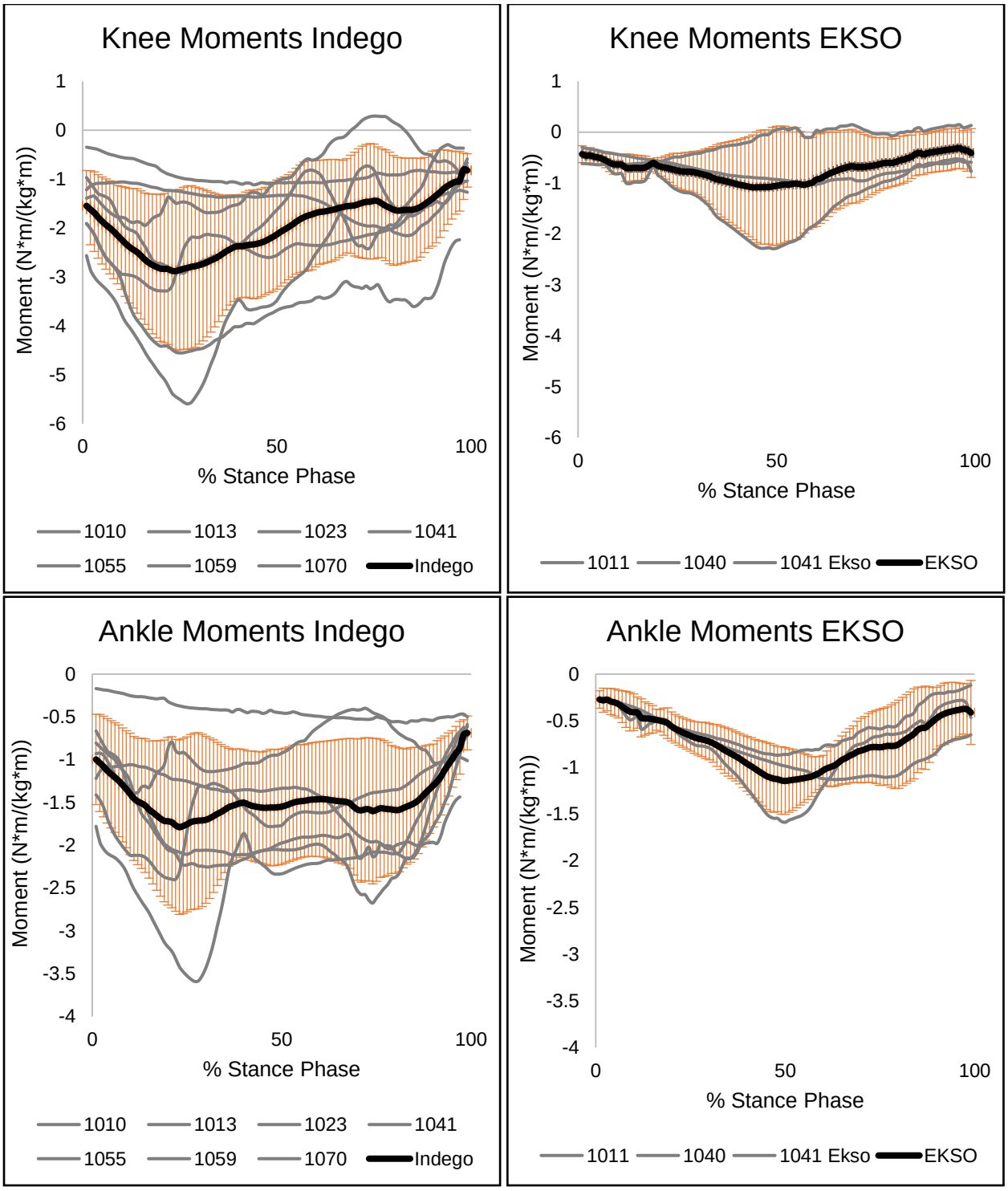

Figure 7: Knee and ankle moments versus stance phase for both exoskeletons

Table 4: Kinetics, kinematics, and temporal parameter averages and t-test results

Group Statistics				
		Exoskeleton		**T-test**
	Dependent Variable (n=Indego / Ekso)	*Indego*	*EKSO*	*p-values*
Forces p=0.371	**Max knee (N/kg) n = 7/3**	11.71 (4.40)	6.66 (0.62)	0.092
	Max ankle (N/kg) n = 7/3	11.49 (4.41)	6.29 (0.65)	0.085
	Peak PRF (N/kg) n=10/4	11.73 (3.83)	8.16 (2.38)	0.112
	Peak PRF loading rate (N/kg/s) n = 10/4	65.81 (50.42)	26.12 (12.63)	0.154
Angles p=0.014	**Knee Range of Motion (degrees) n = 8/4**	69.04 (6.40)	51.03 (3.90)	**0.000**
	Min Knee (degrees) n = 8/4	108.94 (6.69)	115.36 (5.00)	0.123
	Max knee (degrees) n = 8/4	177.98 (2.52)	166.38 (3.50)	**0.000**
	Ankle Range of Motion (degrees) n = 7/3	28.55 (6.21)	16.53 (3.84)	**0.016**
	Min ankle (degrees) n = 7/3	85.06 (5.51)	76.24 (1.28)	**0.029**
	Max ankle (degrees) n = 7/3	113.60 (8.34)	92.78 (2.83)	**0.003**
Moments p=0.400	**Min knee (N*m/(kg*m)) n = 7/3**	-3.06 (1.57)	-1.33 (0.85)	0.115
	Max knee (N*m/(kg*m)) n = 7/3	-0.67 (0.719)	-0.18 (0.285)	0.296
	Min ankle (N*m/(kg*m)) n = 7/3	-2.15 (0.958)	-1.20 (0.363)	0.144
	Max ankle (N*m/(kg*m)) n = 7/3	-0.596 (0.261)	-0.215 (0.083)	**0.043**
Temporal Parameters p=0.028	**Stride time (s) n = 10/5**	2.35 (0.253)	3.42 (0.368)	**0.000**
	stance time (% Stride time) n = 10/5	72.14 (4.97)	74.57 (1.65)	0.314
	swing time (% Stride time) n = 10/5	27.76 (4.84)	25.83 (1.44)	0.407

	Ten meter walking speed (m/s) n = 8/4	0.397 (0.099)	0.264 (0.060)	**0.035**
	Ten meter stride length (cm) n = 8/4	105.04 (20.75)	87.05 (19.74)	0.181
	%Stance Phase of max knee force n = 7/3	54.69 (7.83)	48.00 (10.70)	0.295

Discussion

The therapeutic benefits of exoskeleton walking therapy in participants with spinal cord injuries has been difficult to determine. The overarching question we are interested in is whether the loading on the lower limbs is enough to affect the bone quality of SCI participant. The purpose of this study was to characterize the kinetics and kinematics associated with exoskeleton walking therapy. We assessed these variables using a combination of video footage and pressure sensing insoles to quantify the participant specific kinematics and kinetics. Overall, the two exoskeletons performed slightly differently, with larger ranges of motion and faster walking speeds being achieved with the Indego versus the EKSO. This was associated knee forces of approximately one bodyweight through the lower limbs in the Indego, and about 65% bodyweight using the Ekso. However, the three participants who walked in both exoskeletons did not consistently show lower forces in the EKSO, suggesting that weightbearing may not necessarily differ between the two devices.

Looking at the data overall, during walking there was greater variation in the knee and ankle forces than that of knee and ankle angles. Both exoskeletons include trajectory control of the legs and adjustment of step parameters by a therapist (Moisio et al., 2003). This results in fairly consistent joint angles over time (normalized to the length of the stance phase). However, the net joint force calculations relied on data from pressure-sensing insoles. The insoles measured the forces on the plantar surface of the participant's feet, and thus reflect the loading actually experienced by their body. However, all participants walked with an assistive device, typically a walker, and the amount of weight transmitted through that device varied over

the gait cycle and from person to person. This may explain some of the between-participant variation we observed in net joint forces.

The net joint moments in the ankle were smaller than those observed in able-bodied walking using both exoskeletons. The net joint moments at the ankle were 77% smaller and 87% smaller in the Indego and EKSO respectively. Both exoskeletons have passive spring mechanisms at the ankle, which limits the range of motion and allows for some elastic energy storage and return. At the knee, the net joint moments still varied from that experienced during able-bodied walking, but using the Indego, the net moments were 9-22% greater, whereas in the EKSO, the net moments were and 48-54% smaller than able-bodied walking (D'Lima et al., 2012). The moments that we report here reflect the total moment that must be applied to the participant's joint to produce the observed motion. However, unlike in able-bodied gait, individuals with complete SCI have no voluntary muscle contraction and rely completely on the exoskeleton actuators to generate the observed motion. Thus, while joint contact forces and the resulting skeletal loading are typically 2.5-2.8 bodyweights during able-bodied walking due to muscles acting with a small moment arm (Shields & Dudley-Javoroski, 2006), we estimate that the joint contact forces at the knee for these participants are closer to 1 bodyweight. This still may be sufficient to have a positive effect on bone. For example, isometric ankle plantarflexion with electrical stimulation was osteogenic with approximately 1 bodyweight of force across the distal tibia (Schache et al., 2011). The parent clinical trial data will ultimately address the degree to which exoskeleton walking therapy can benefit bone health in this population.

The Indego resulted in slightly larger net joint forces and rates of force application at the ankles and knees compared to the EKSO. At the same time, walking speed for the EKSO was significantly slower (25 cm/s versus 44 cm/s). Since ground reaction and joint forces increase with increasing speeds (Rodríguez-Fernández et al., 2021), it's possible that much of the between-exoskeleton differences arise from walking speed. However, the two exoskeletons also have different control systems, which may influence kinetics. The EKSO initiates a step in response to a side-to-side weight shift or a push-button on a crutch. In contrast, the Indego initiates a step in response to a forward lean and anterior shift in center of pressure (Turner & Robling, 2003). A forward leaning configuration requires a longer step and larger

ground reaction force to maintain stability. Although our pressure sensing insole system was unable to measure shear forces, it is likely that the longer Indego steps included a greater frictional shear component as well.

This study had several limitations. Because only one individual had complete data from both exoskeletons, our between-exoskeleton comparison was not as robust as would be ideal. Additionally, there were uneven cohort sizes between both exoskeletons. In those who did have paired data, there were no consistent differences in the PRFs recorded in each of the exoskeletons. Another limitation to this study is that the video and insole data were collected at the end of the six months of walking therapy. It is likely that gait kinetics and kinematics changed as the training progressed, both by changing mobility aids and reducing the reliance on the aid during walking. However, the data were collected at the same point during gait training for all participants. Finally, the pressure sensing insoles themselves may not have been as accurate during this type of assisted walking as they are during able-bodied walking. These insoles do not have 100% coverage of the sole of the foot, and rely on an algorithm to translate plantar pressure into net force. However, because the exoskeleton lifts the foot during swing phase, the insole is never entirely unloaded as it would be during able-bodied walking.

In summary, this study characterized the kinematics and kinetics associated with exoskeleton walking therapy in individuals with chronic SCI. Individuals with SCI experience a decrease in bone mass and strength and exoskeleton walking therapy has the possibility of loading the lower extremities. We calculated the net forces and moments experienced at the ankle and knee during exoskeleton walking therapy using two separate exoskeletons. The forces generated during walking therapy were lower than able-bodied walking, but may potentially be osteogenic, based on prior studies with similar loading being applied to bone. Additionally, the net knee moments using the Indego were slightly higher than that experienced during able-bodied walking. Thus, certain aspects of exoskeleton therapy could resemble able-bodied walking. The results of this study have the potential to allow clinicians to tailor walking therapy to individual patients, and better understand how exoskeleton therapy loads the lower extremities.

Chapter 5: Establishing the relationship between exoskeleton walking therapy loading dose and changes in integral bone mineral content

Introduction

Bone's ability to remodel can be induced by the mechanical loads it experiences. When loads are removed from the bone altogether, as can be the case with SCI, the bone strain decreases and remodeling can be shifted in the direction of losing bone faster than bone is being rebuilt. This leads to SCI-induced osteoporosis, making the bones weak and fracture prone. By adding mechanical loading back to the bone, there is the potential that bone remodeling could be shifted in the other direction, towards the formation of bone instead of higher levels of resorption.

Prior research has demonstrated that different activities, and their frequency, and duration have an impact on how bone responds to them. Although various theoretical relationships have been proposed to predict osteogenic response, they all have real-world limitations. One method proposed to predict changes in bone mass based on exercise is the Osteogenic Index using loading cycles, and exercise intensity (Turner & Robling, 2003). Similarly, self-reported questionnaires like the bone specific physical activity questionnaire (BPAQ), and the bone loading history questionnaire (BLHQ) use block recordings of activity and the duration of the activity over an individual's lifespan. The activities are characterized based on previously collected ground reaction force (GRF) data to determine the loading on the bones, overall (Dolan et al., 2006). The problem with these measures is that prospective animal studies to look at the predictability of these measures all use strain as a measure of bone loading, whereas human studies do not. This disconnect could affect the predictive ability of the models as there is variation between individual bone structure, resulting in strains that span over a 5-fold range for a given applied force (Mancuso et al., 2018). Although these calculations and questionnaires can help us understand how the quality of bone is affected by loading from specific activities, it is unclear how this could help predict changes in SCI-induced bone loss as a result of loading.

Even though there isn't a complete understanding of how loading from different activities affects SCI-induced loss of bone mass, there are several different therapies that have been tested to treat this bone loss, including functional electrical stimulation (FES) rowing and cycling. A newer method to load the lower limbs is to use exoskeleton walking therapy which allows individuals with SCI to walk powered by motors and servos connected to an external frame. Given that the users are walking upright and supporting their own body weight, there is the potential that the forces through the lower limbs could be higher than that of other physical interventions. FES rowing is a whole-body exercise, but studies have shown that there is not a large amount of force traveling through the lower limbs, even though this could be altered through changes in positioning and speed (Draghici et al., 2017; Fang et al., 2021). Numerous studies have shown improvements in BMD following FES cycling, but when FES cycling therapy was stopped, the therapeutic effects immediately were halted or reversed (Frotzler et al., 2008; Lai et al., 2010; Mohr et al., 1997). Given that exoskeleton walking therapy allows the users to support their own body weight, unlike in FES rowing or cycling, there is a greater likelihood that the loading will be higher in the lower limbs during walking therapy.

The purpose of this study is to assess the relationship between candidate measures of loading dose and the change in iBMC of the proximal tibia and distal femur following six months of exoskeleton walking therapy. We hypothesized that there would be a positive relationship between the loading dose and the change in iBMC in the tibia and femur.

Methods

Overview

As part of an ongoing clinical trial, CT scans were acquired in participants before and after 6 months of exoskeleton walking therapy. QCT analysis was used to quantify changes in iBMC in various regions of the proximal tibia and distal femur. We also calculated participant-specific measures of bone strength using QCT in both the tibia and the femur. These measures of bone strength were combined with the number of steps each individual took and the average plantar loading rate for each step to calculate a family of

participant-specific loading dose measures. The loading dose measures were then compared to the prospectively measured changes in iBMC within different regions to determine the degree to which they were related to one another.

Participants

Individuals with spinal cord injury were recruited as part of a larger ongoing clinical trial, the purpose of which is to evaluate skeletal benefits from regular exoskeleton assisted walking therapy (NCT02533713). To enroll in the trial, individuals have to be AIS-A or AIS-B, 3-10 years post-injury, free of known cardiovascular disease, and 40 years or younger. Additionally, participants must have complete thoracic SCI (T3-T12), be between 158-188 cm in height, weight under 100kg, and have a Modified Ashworth Scale (MAS) score of less than 3 in both legs, and have enough strength in the upper body to complete sit to sit transfers. The present study included 13 participants (12 male and 1 female, age: 36.2 ± 8.6 years, height: 179.0 ± 8.0 cm, mass: 79.1 ± 13.08 kg). All participants gave written informed consent to participate in this institutionally approved research study.

As part of the clinical trial, each participant was assigned to walking therapy in an exoskeleton for three hours per week, for six months. All walking therapy was supervised by trained physical therapists and occurred within the PEAK Center at Craig Rehabilitation Hospital (Englewood, CO). The majority of the therapy sessions were performed using an Indego exoskeleton (Indego; Parker Hannifin, Cleveland, OH); however, some participants also used an Ekso exoskeleton (ekso Bionics, Richmond, CA) for some sessions.

Pressure Insole and Exoskeleton Data

To obtain a measure of how much loading the users were experiencing in their lower limbs, Orpyx (Orpyx LogR, Orpyx, Calgary, Alberta, Canada) pressure sensing insoles were used for nine participants during their walking therapy. This is the same subset of participants from Chapter 4 who took part in the video gait data collection. The insole collected the magnitude of the plantar reaction force over time. The peak loading rate (N/s) was determined by averaging the change in force over the change in time for

multiple loading cycles for each participant. Both exoskeletons recorded the total number of steps for each walking therapy session for each participant.

CT Scans

CT scans were taken of both legs for each participant (Revolution CT, GE Medical Systems; pixel resolution 0.352mm, slice thickness 1.25mm, 100mA s, 120kVp, 30cm scan length for 15cm each of distal femur and proximal tibia) at zero (baseline scans), six (second), and twelve (third) months after the trial began. In each scan, a calibration phantom with known hydroxyapatite concentration was placed in between the legs of each individual (custom made calibration phantom standards for 0, 400, and 800 mg HA/cm^3) (Figure 1). The phantoms were used to convert the CT Hounsfield units to bone density for each scan.

CT Alignment

The distal femur and proximal tibia were analyzed and aligned separately. Baseline CT images were manually aligned along the longitudinal axes of the femur and the tibia using Mimics (Materialise, Leuven, Belgium). Second and third scans were registered using a proven registration method demonstrated by Edwards et a. with a combination of Mimics and Matlab software (MathWorks, Natick, MA, USA) (Edwards et al., 2013). The epiphysis, metaphysis, and diaphysis were marked as 10, 20, and 30% of the total length of the bone from the distal femur and proximal tibia. Femur and tibia lengths were calculated using participant heights and anthropometric calculations from Winter (Lang et al., 2006).

QCT Mineral Analysis

The relationship between equivalent bone density and Hounsfield units was established using a linear equation developed using the calibration phantoms. The periosteal surface was identified using a density threshold of 0.15g/cm^3 (Figure 2). In regions where the cortical shell was thin due to the bones having a lower density, primarily at the epiphysis and metaphysis, manual identification of the periosteal surface was performed (Figure 3). Integral, cortical, and trabecular regions were identified using methods similar to Edwards et al. (Lang et al., 2004). Integral regions were comprised of all voxels within the periosteal surface. Trabecular regions were identified using a 3.5mm in plane erosion from the integral region. The cortical region was selected using a Boolean operation subtracting the trabecular region from

the integral region. The integral bone volume (cm^3) was calculated as the total volume within the periosteal surface by multiplying the number of voxels by their known size using Matlab 2019 (Simulink, Natick, MA). We also calculated total femoral and tibial iBMC by averaging the density of each voxel and multiplying by the integral bone volume, and the iBMC at the epiphysis, metaphysis, and diaphysis.

Bone Strength Calculations

To obtain participant-specific bone strength metrics used in the loading dose calculations, we used Matlab to calculate various measures of bone strength including the buckling ratio of the entire tibia, bending strength index, and compressive strength index of the epiphysis, metaphysis, and diaphysis of the tibia. The equations used can be found in Table 5. The epiphysis, metaphysis, and diaphysis of the tibia were defined as 10, 20, and 30% of the total length of the tibia from the proximal most point of the tibia.

Table 5: Bone strength calculations for loading dose

Measurement	**Description**	**Equation**
Compressive strength index CSI (g^2/cm^4)	Index based on average bone mineral density and average cross-sectional area of region of interest (Cheng et al., 2007)	$$CSI = BMD^2 * CSA$$
Bending strength index BSI (cm^3)	Is the sum of the effective moments of inertia divided by the diameter of a circular cross-section equivalent area (Lang et al., 2004)	$$BSI = \frac{I_X + I_Y}{W}$$ $$I_X = \frac{1}{e_b}\sum_i e_i * (x_i - \bar{x})^2 * area_{voxels}$$ $$I_Y = \frac{1}{e_b}\sum_i e_i * (y_i - \bar{y})^2 * area_{voxels}$$ $$W = 2 * \sqrt{\frac{CSA}{\pi}}$$
Buckling ratio BR	The ratio of the cortical thickness index to the effective bone half width(Cheng et al., 2007)	$$BR = iCThi/iBTHi$$ $$iCThi = 0.5 * \left[\sqrt{\frac{\frac{iBV_{reg}}{length_{reg}}}{\pi}} - \sqrt{\frac{\frac{iBV_{reg} - cBV_{reg}}{length_{reg}}}{\pi}}\right]$$ $$iBThi = 0.5 * \sqrt{\frac{\frac{iBV_{reg}}{length_{reg}}}{\pi}}$$

BMD : bone mineral density
CSA : cross-sectional area

$area_{voxel}$: area of each voxel in the transverse plane
e_b : cortical bone elastic modulus
e_i : equivalent elastic modulus of each voxel
x_i, y_i : coordinates of the i^{th} voxel
$\bar{x}, \bar{y}$: elastic modulus weighted centroid
W : diameter of a circular cross-section equivalent area
I_x, I_y : effective polar moments of intertia
iBV_{reg} : integral bone volume of region of interest
$length_{reg}$: length of region of interest
cBV_{reg} : cortical bone volume of region of interest

Loading Dose Calculations

Participant specific loading dose calculations were developed based on previously published equations to describe bone loading stimulus using loading intensity, cycles, and a measure of bone strength (Troy et al., 2020; Turner & Robling, 2003) (for example, Osteogenic Index [ref] and a metric of loading dose defined by Troy et. Al [ref my JBMR paper 2020]). Our initial dose included a linear combination of the number of steps that each individual took in the exoskeleton, the peak loading rates, and measures of bone strength at each region of the tibia and femur, or for just the tibial or femoral metaphysis in the case of buckling ratio (Equation 5).

Loading dose = (total steps*loading rate)/bone strength measure (5)

For the individuals who did not have pressure sensing insole data, we averaged the normalized peak loading rate from those who did have Orpyx data, and multiplied the normalized loading rate by the individual participant weights. We calculated several candidate measures of loading dose using the different bone strength measures. From these measures, we calculated correlations between the candidate measures of loading dose and the primary outcome measure, change in iBMC within the relevant anatomy. Both Pearson and Spearman's (rank-ordered) correlations were calculated, to account for the small sample size. Femur-based strength measures were used for dose comparisons with femur bone, and tibia-based strength measures were compared with tibia changes. All statistical calculations were completed using SPSS v. 23 (IBM, Armonk, NY).

Results

In this study, we analyzed data from six left, and nine right tibias and femurs from nine participants. All correlations were higher in the femur than in the tibia. The highest Pearson correlation coefficient was between the changes in total iBMC in the femur and the bone loading dose calculation using the femoral epiphyseal BSI (Table 7). The highest Spearman's rho correlation coefficient was between the total iBMC changes in the femur and the loading dose calculation using the femoral metaphyseal BSI. In the tibia, the Pearson correlations between the loading doses and the changes in iBMC were all negative and insignificant. The loading dose calculation using the tibial diaphyseal CSI had the highest Spearman's rho correlation coefficient, but it was still insignificant. Additionally, the relationships between the loading dose calculations of the same bone were linearly related aside from the tibial and femoral epiphyseal CSI.

Table 6: Participant-specific loading dose calculations

						Tibial bone strength metrics		Tibial loading dose	
Sub	**Side (1 = left, 2 = right)**	**Weight (kg)**	**Total Steps**	**Peak Loading Rate (N/s)**	**Peak Loading Rate Normalized (N/kg/s)**	**metBR**	**epiCSI (g^2/cm^4)**	**metBR (steps*N/kg/s)**	**epiCSI (steps*N/kg/s/(g^2/cm^4))**
1001	1	91.85	168897	5661.32	61.64	0.14	0.39	684.87	247.37
	2					0.13	0.37	726.18	255.93
1010	1	105.78	104734	1596.79	15.10	0.14	0.51	119.80	32.48
	2					0.16	0.37	106.33	45.56
1011	1	82.78	145354	5093.03	61.64	0.22	0.16	334.24	462.62
	2					0.17	0.19	432.37	397.54
1013	2	53.44	158047	7973.13	149.21	0.15	0.08	856.26	1655.55
1018	2	79.00	159326	1820.00	23.04	0.10	0.09	280.41	307.09
1019	2	73.94	111901	4557.21	61.64	0.12	0.20	428.44	259.91
1023	1	67.87	133840	7368.33	108.56	0.14	0.13	690.36	747.70
	2					0.14	0.13	727.24	735.28
1028	1	70.82	161163	4365.35	61.64	0.13	0.07	557.17	940.54
	2					0.13	0.07	537.74	1063.30
1040	1	82.17	102090	3065.45	37.31	0.13	0.21	239.43	150.90

	2					0.11	0.17	285.92	180.50
1041	1	84.90	154620	3845.26	45.29	0.15	0.46	386.14	130.28
	2					0.16	0.42	376.79	139.93
1059	1	66.33	172397	7275.00	109.68	0.11	0.09	1183.46	1377.20
	2					0.11	0.10	1118.45	1282.13
1064	1	80.36	186282	4953.00	61.64	0.13	0.06	686.48	1633.83
	2					0.13	0.07	716.22	1297.44
1070	1	87.62	175026	3318	37.87	0.18	0.47	320.53	123.31
	2					0.18	0.50	321.88	117.23

*loading dose measures divided by 10^7

Table 7: Femoral iBMC change and loading dose correlations

Bone strength measure in loading dose calculation	Pearson Correlation with respect to iBMC change in femur	Spearman's rho Correlation with respect to iBMC change in femur
Femoral metaphysis buckling ratio	0.265	0.263
Femoral epiphyseal CSI	0.362	0.272
Femoral metaphyseal CSI	0.291	0.319
Femoral diaphyseal CSI	0.296	0.259
Femoral epiphyseal BSI	***0.457**	0.327
Femoral metaphyseal BSI	***0.409**	0.345
Femoral diaphyseal BSI	***0.437**	0.301

*indicates significant at α = 0.05

Table 8: Tibial iBMC change and loading dose correlations

Bone strength measure in loading dose calculation	Pearson Correlation with respect to iBMC change in tibia	Spearman's rho Correlation with respect to iBMC change in tibia
Tibial metaphysis buckling ratio	-0.143	0.019
Tibial epiphyseal CSI	-0.076	-0.074
Tibial metaphyseal CSI	-0.140	0.041
Tibial diaphyseal CSI	-0.102	0.116
Tibial epiphyseal BSI	-0.084	0.046
Tibial metaphyseal BSI	-0.066	0.078

Tibial diaphyseal BSI	-0.048	0.067

*indicates significant at α = 0.05

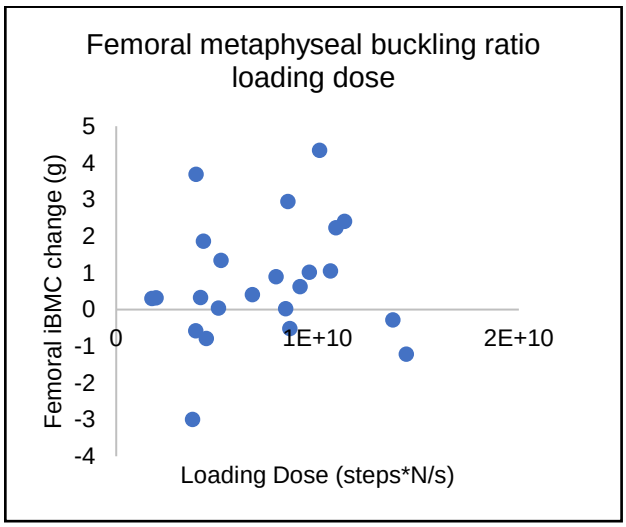

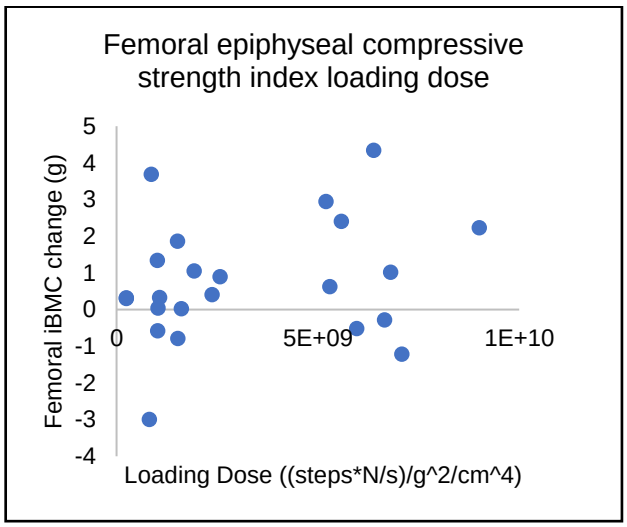

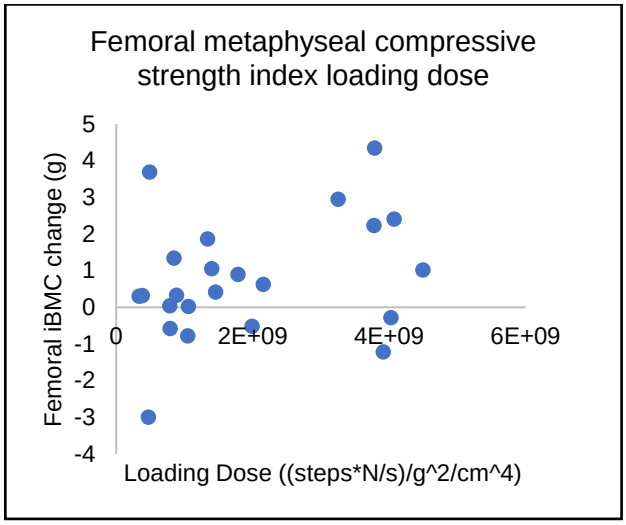

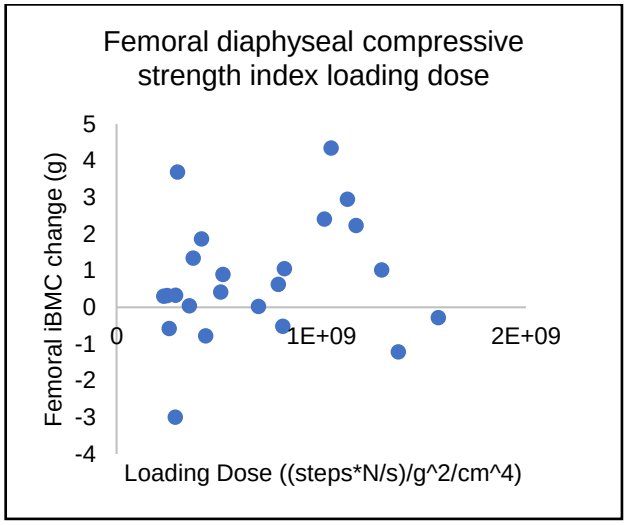

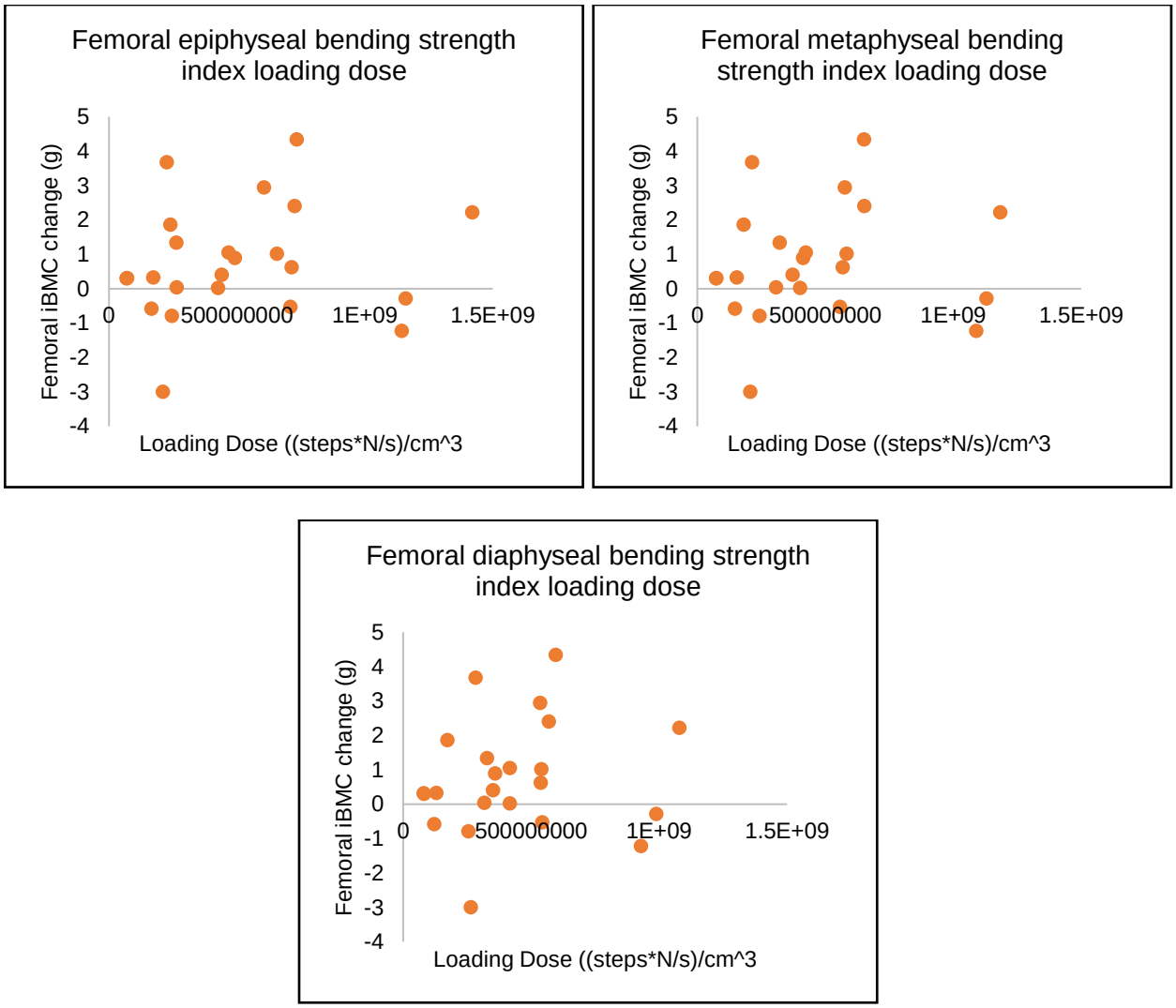

Figure 8: Femoral iBMC change versus loading dose calculations (orange indicates significant Pearson's correlation coefficients at the α = 0.05 level)

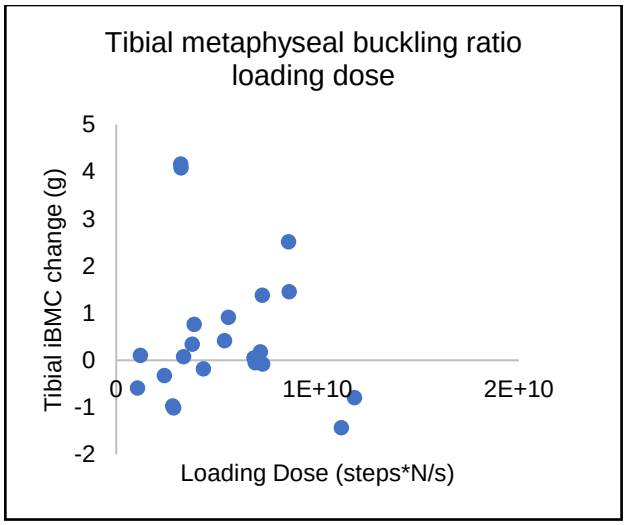
Tibial metaphyseal buckling ratio loading dose
Tibial iBMC change (g)
5
4
3
2
1
0
-1
-2
0
1E+10
2E+10
Loading Dose (steps*N/s)

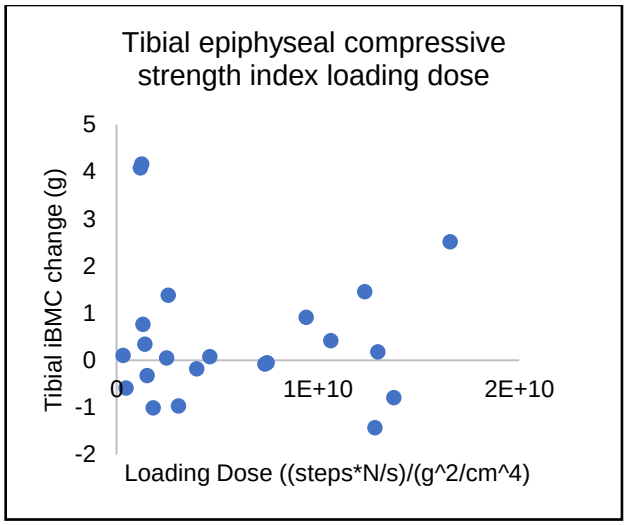
Tibial epiphyseal compressive strength index loading dose
Tibial iBMC change (g)
5
4
3
2
1
0
-1
-2
0
1E+10
2E+10
Loading Dose ((steps*N/s)/(g^2/cm^4)

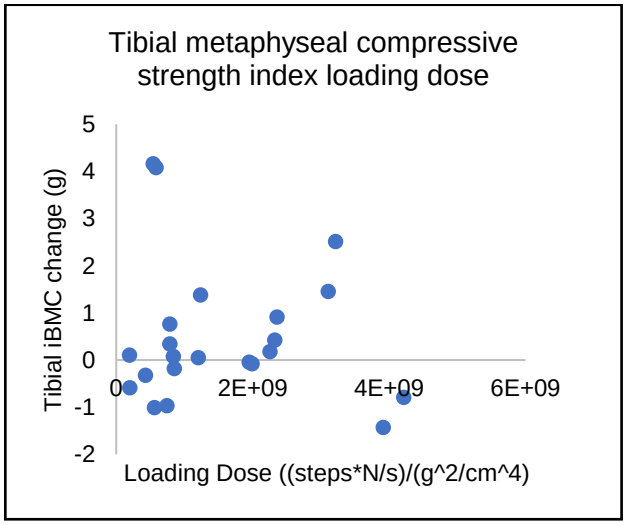
Tibial metaphyseal compressive strength index loading dose
Tibial iBMC change (g)
5
4
3
2
1
0
-1
-2
0
2E+09
4E+09
6E+09
Loading Dose ((steps*N/s)/(g^2/cm^4)

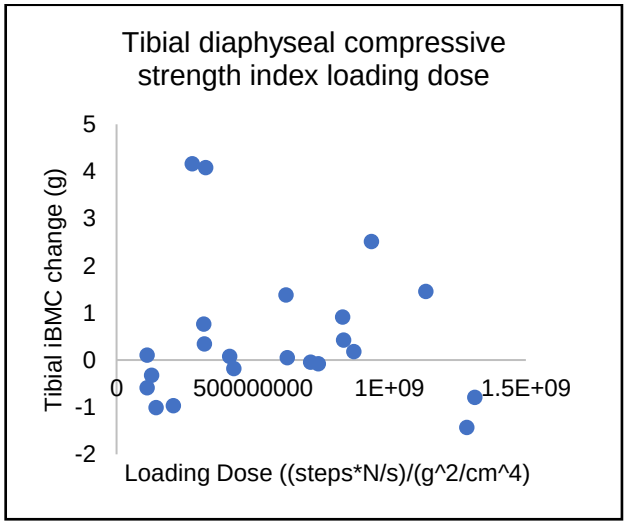
Tibial diaphyseal compressive strength index loading dose
Tibial iBMC change (g)
5
4
3
2
1
0
-1
-2
0
500000000
1E+09
1.5E+09
Loading Dose ((steps*N/s)/(g^2/cm^4)

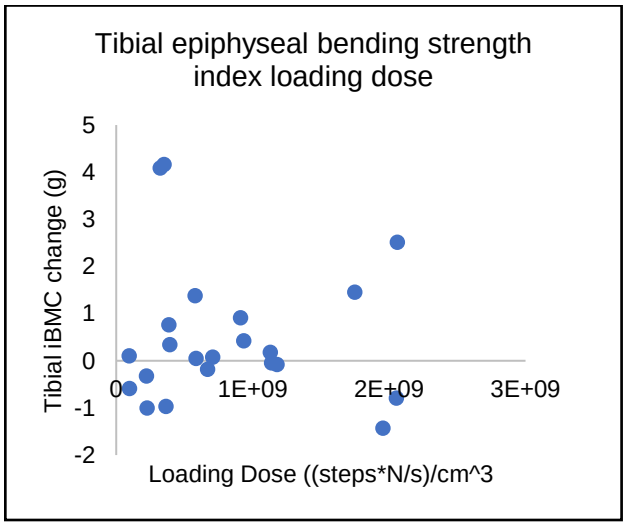
Tibial epiphyseal bending strength index loading dose
Tibial iBMC change (g)
5
4
3
2
1
0
-1
-2
0
1E+09
2E+09
3E+09
Loading Dose ((steps*N/s)/cm^3

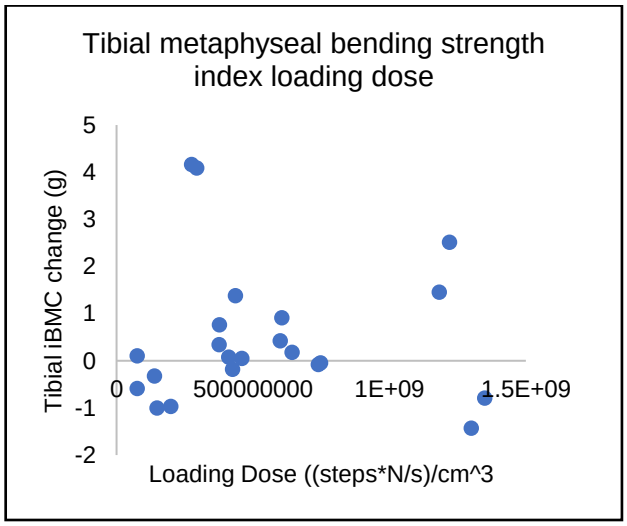
Tibial metaphyseal bending strength index loading dose
Tibial iBMC change (g)
5
4
3
2
1
0
-1
-2
0
500000000
1E+09
1.5E+09
Loading Dose ((steps*N/s)/cm^3

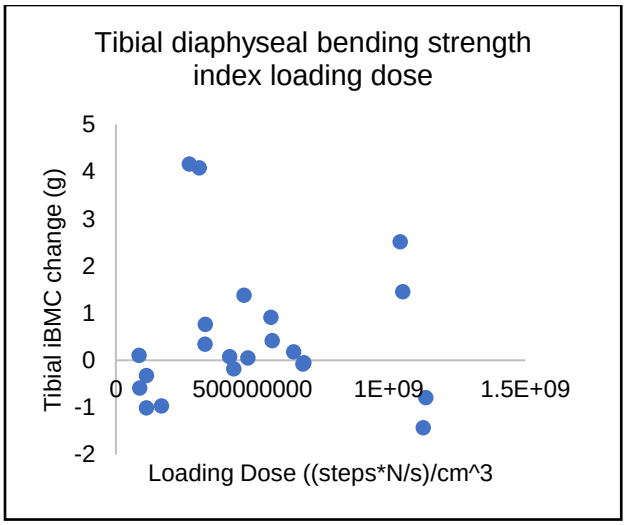

Figure 9: Tibial iBMC change versus loading dose calculations (orange indicates significant Pearson's correlation coefficients at the α = 0.05 level)

Discussion

Mechanical loading of the lower limbs in individuals with SCI has the potential to improve bone quality. The purpose of this study was to assess how the changes in bone quality were related to the total amount of loading on the bone following exoskeleton walking therapy. We used QCT analysis and data recording from the exoskeleton and pressure sensing insoles to calculate the change in total iBMC of the tibia and the femur and participant specific loading dose measures. Overall, measures of loading dose had a higher positive correlation to the change in the iBMC in the femur than the tibia. The only correlations that were significant were the Pearson's correlations in the femur with loading doses using the BSI of different femoral regions ($p \leq 0.05$). The highest correlation was observed between iBMC changes and loading dose calculations using the femoral epiphyseal BSI. This suggests a positive relationship between the changes in the iBMC and the loading associated with exoskeleton therapy.

Several studies have demonstrated the ability of physical therapy techniques, such as FES rowing and cycling to induce changes in bone in those with SCI. Very few studies exist that assess how exoskeleton walking therapy can impact bone quality in the lower extremities for individuals with SCI, and none have included a method for analyzing dose-dependent responses (Morse et al., 2019). Calculations, like the osteogenic index, BLHQ, and BPAQ can provide some indication of how a bone may respond to mechanical

loading, but very little human data is available. Dose-dependent responses in humans have, however, been calculated in FES rowing studies. Morse et al. following an FES rowing clinical trial observed a dose-dependent increase in the cortical thickness index and BR after rowing (Lambach et al., 2020). Lambach et al. conducted a prospective study on FES rowing and noted a similar bone stimulus dependent response with the change in trabecular BMD of the femur (Lambach et al., 2020). The bone stimulus used a combination of the number of loading cycles for each individual, and participant-specific peak foot force and initial BMC. This bone stimulus calculation is similar to what we proposed in this study as the participant-specific bone loading dose, using the total number of cycles, a force metric, and a measure of bone quality or strength. These studies are helpful for beginning to understand the relationship between loading dose and bone adaptation, but no prospective study prior to this has been done to assess that same relationship using exoskeleton walking therapy.

Although the correlations observed suggest a relationship between changes in iBMC and loading dose, there were several limitations to this study. There was a relatively small number of individuals with complete data during this time. Being an ongoing clinical trial, more data can be added to the calculations following this procedure in the future. Additionally, not all individuals in this trial had pressure sensing insole data collected, so the average of available loading rates were used in its place. We suggest that pressure sensing insole data be added to the data collected during the remaining participants in the clinical trial to collect more pressure sensing insole data for loading dose calculations.

To summarize, this study highlighted the potential for a relationship between changes in the bone and measures of loading dose during exoskeleton therapy. The positive correlations using the bone strength metrics of the femur suggest that bone responds to exoskeleton walking therapy in a dose-dependent manner. The results of this study can inform decisions regarding how much walking therapy is needed to induce changes in bone physiology.

Chapter 6: Discussion

The therapeutic benefits associated with exoskeleton walking therapy for individuals with SCI are not completely understood. Few studies have assessed the changes in bone physiology as a result of using this type of therapy. In this thesis, we established that there is a significant increase in the iBMC of the femoral and tibial epiphyses and throughout the total femur following walking therapy. The iBMC was selected as a measure of improved bone remodeling because it provides a wholistic understanding of the total amount of bone within a given region of interest. When an SCI occurs and loading of the lower limbs is halted, the bone is shifted in the direction of more resorption, causing severe bone loss. The positive change in the iBMC could help understand whether or not exoskeleton walking therapy sufficiently loads the lower limbs to induce physiological changes in the bone.

Although exoskeleton walking therapy has been used with individuals with SCI, the kinematics and kinetics between different types of exoskeletons has not been thoroughly characterized and compared. This research calculated the kinematics, kinetics, and temporal parameters associated with several individuals during exoskeleton walking therapy. Although the kinematics and kinetics associated with the two exoskeletons were different, the only significant changes were in the temporal parameters and the kinematics. The kinetics using the EKSO exoskeleton were smaller than that seen in the Indego, but the differences between the two were not significant, indicating that there should be no significant loading in the lower limbs between the exoskeletons. Although the forces were smaller than those seen in able-bodied walking, other studies have shown an osteogenic response to loading to forces of a similar magnitude.

Characterizing the kinetics and kinematics associated with exoskeleton walking therapy can help us understand whether or not bones are being loaded enough for an osteogenic response, but there are currently no calculations to predict the degree of response in SCI-osteoporotic bone. We used participant-specific metrics and measurements to create several candidate loading dose measures. When the changes in the iBMC of the tibia and femur were compared to the loading dose calculations, there were moderate positive correlations with measures of loading dose using femur BSI at different bone regions. All

correlations were higher in the femur than in the tibia. The loading dose calculation with the highest correlation used the tibial diaphyseal BSI as the bone strength metric. In the femur, the loading dose using the epiphyseal BSI had the highest correlation.

There were several limitations with this research, namely the small sample size. As aforementioned, this clinical trial is ongoing, and data are continuing to be collected from participants. This data can then be implemented into the methods presented here to add to increase the statistical power associated with the comparisons made in the studies. It is also important to note that the majority of the participants in this study are male; however, this is representative of the SCI population as a whole as the most individuals with SCI are male.

Overall, the goal of this thesis was to determine the degree to which exoskeleton walking therapy increased iBMC of the distal femur and proximal tibia in a dose-dependent manner. Because walking therapy can vary in duration, speed, force, and reliance on walking aids, participant-specific measures were essential to compare the changes seen in the iBMC. The loading dose measures we developed are a first attempt to calculate a cumulative amount of loading and normalized the loading with respect to patient specific metrics of bone strength from QCT analysis. However, there are other plausible formulations for this metric that should be explored. These loading dose calculations can help us understand to what degree the changes in bone mass in the femur and tibia are related to exoskeleton walking therapy, or other causes. The moderate positive correlation between bone changes and the loading dose calculations using measures of femur strength support the overall hypothesis that exoskeleton walking therapy can improve iBMC of regions of the distal femur and proximal tibia in a dose-dependent manner. Although we cannot directly conclude that the use of the exoskeleton is the direct cause of the increase in bone mass, this thesis can help inform decisions regarding the use of exoskeleton walking therapy.

Conclusion and Future Directions

In this thesis, we investigated exoskeleton walking therapy's ability to induce an osteogenic response in the femur and tibia in those with SCI. After walking therapy, participants experienced significant increases in iBMC in the epiphyseal region of the femur and tibia and in the total femur. Despite using two different exoskeletons during walking therapy, there were no significant differences in the forces in the lower extremities, indicating that exoskeleton type should not affect the overall goal of loading the lower limbs. When the changes in the iBMC are compared to the total amount of walking done by each individual, and participant-specific loading rate and bone strength, there is a positive correlation between the two measures. This research is an important step in understanding how and why exoskeleton therapy could be beneficial in SCI populations.

Further research should continue to look at changes between iBMC of the tibia and femur using the data that are still being collected from the clinical trial. Changes in iBMC as well as different bone strength metrics with additional data points can be added to the paired t-test from Chapter 3 to improve statistical power and determine if there could be any relationship between exoskeleton walking therapy and changes in bone strength. Measures of loading dose using force intensity metrics, other than peak loading rate, should be calculated and compared to iBMC changes. Additionally, further comparisons of different characteristics of individuals who did gain bone to those who did not gain bone mass can be made, including type of mobility aid used during therapy. To avoid averaging kinetic data, pressure sensing insole data should be collected during walking therapy for each individual in order to continue calculating participant-specific loading dose measures. Different loading metrics, aside from peak loading rate from the pressure sensing insoles should be investigated in addition to calculating the current loading dose measures as new participant data are collected. This could provide more insight into how different kinetics associated with exoskeleton walking therapy are related to changes in bone mass. In summary, this research provided important information regarding how weakened bone could adapt to mechanical loading.

References:

Spinal Cord Injury Facts and Figures at a Glance Since 2015 Since 2015 Incomplete Tetraplegia Incomplete Paraplegia Complete Paraplegia Complete Tetraplegia Normal. (2018). www.msktc.org/sci/model-system-centers.

Bach Baunsgaard, C., Vig Nissen, U., Katrin Brust, A., Frotzler, A., Ribeill, C., Kalke, Y. B., León, N., Gómez, B., Samuelsson, K., Antepohl, W., Holmström, U., Marklund, N., Glott, T., Opheim, A., Benito, J., Murillo, N., Nachtegaal, J., Faber, W., & Biering-Sørensen, F. (2018). Gait training after spinal cord injury: Safety, feasibility and gait function following 8 weeks of training with the exoskeletons from Ekso Bionics article. *Spinal Cord*, *56*(2), 106–116. https://doi.org/10.1038/s41393-017-0013-7

Bar-Shavit, Z. (2007). The Osteoclast: A Multinucleated, Hematopoietic-Origin, Bone-Resorbing Osteoimmune Cell. *Journal of Cellular Biochemistry*, *102*, 1130–1139. https://doi.org/10.1002/jcb.21553

Battaglino, R. A., Lazzari, A. A., Garshick, E., & Morse, L. R. (2012). Spinal cord injury-induced osteoporosis: Pathogenesis and emerging therapies. *Current Osteoporosis Reports*, *10*(4), 278–285. https://doi.org/10.1007/s11914-012-0117-0

Bauman, W. A., & Cardozo, C. P. (2015). Osteoporosis in Individuals with Spinal Cord Injury. *PM and R*, *7*(2), 188–201. https://doi.org/10.1016/j.pmrj.2014.08.948

Beggs, L. A., Ye, F., Ghosh, P., Beck, D. T., Conover, C. F., Balaez, A., Miller, J. R., Phillips, E. G., Zheng, N., Williams, A. A., Aguirre, J., Wronski, T. J., Bose, P. K., Borst, S. E., & Yarrow, J. F. (2015). Sclerostin inhibition prevents spinal cord injury-induced cancellous bone loss. *Journal of Bone and Mineral Research*, *30*(4), 681–689. https://doi.org/10.1002/jbmr.2396

Berger, A. (2002). Bone mineral density scans. *BMJ*, *325*(7362), 484. https://doi.org/10.1136/bmj.325.7362.484

Biering-Sorensen, B., & Schaadt, O. (1990). Longitudinal study of bone mineral content in the lumbar spine, the forearm and the lower extremities after spinal cord injury. *European Journal of Clinical Investigation*, *20*, 330–335.

Biering-Sørensen, F., Hansen, B., & Lee, B. S. B. (2009). Non-pharmacological treatment and prevention of bone loss after spinal cord injury: A systematic review. *Spinal Cord*, *47*(7), 508–518. https://doi.org/10.1038/sc.2008.177

Bonewald, L. F. (2007). Osteocytes as dynamic multifunctional cells. *Annals of the New York Academy of Sciences*, *1116*, 281–290. https://doi.org/10.1196/annals.1402.018

Bryson, J. E., & Gourlay, M. L. (2009). REVIEW Bisphosphonate Use in Acute and Chronic Spinal Cord Injury: A Systematic Review. In *J Spinal Cord Med* (Vol. 32, Issue 3).

Carbone, L. D., Chin, A. S., Burns, S. P., Svircev, J. N., Hoenig, H., Heggeness, M., & Weaver, F. (2013). Morbidity following lower extremity fractures in men with spinal cord injury. *Osteoporosis International*, *24*(8), 2261–2267. https://doi.org/10.1007/s00198-013-2295-8

Chantraine, A., Nusgens, B., & Lapiere, C. M. (1986). Bone remodeling during the development of osteoporosis in paraplegia. *Calcified Tissue International*, *38*(6), 323–327. https://doi.org/10.1007/BF02555744

Cheng, X., Li, J., Lu, Y., Keyak, J., & Lang, T. (2007). Proximal femoral density and geometry measurements by quantitative computed tomography: Association with hip fracture. *Bone*, *40*(1), 169–174. https://doi.org/10.1016/j.bone.2006.06.018

Cheu, J., Kirch, R., Silvestris, S., Sziy, R., & Troy, K. (2018). *Design of a Wearable Sensor System for the Estimation of Lower Limb Joint Loading*. http://www.wpi.edu/academics/ugradstudies/project-learning.html.

de Bakker, C. M. J., Tseng, W. J., Li, Y., Zhao, H., & Liu, X. S. (2017). Clinical Evaluation of Bone Strength and Fracture Risk. In *Current Osteoporosis Reports* (Vol. 15, Issue 1, pp. 32–42). Current Medicine Group LLC 1. https://doi.org/10.1007/s11914-017-0346-3

Dejong, G., Tian, W., Hsieh, C., Junn, C., Karam, C., Ballard, P. H., Smout, R. J., Horn, S. D., Zanca, J. M., Heinemann, A. W., Hammond, F. M., & Backus, D. (2013). Rehospitalization in the First Year of Traumatic Spinal Cord Injury After Discharge From Medical Rehabilitation. *Archives of Physical Medicine and Rehabilitation*, *94*(4), S87–S97. https://doi.org/10.1016/j.apmr.2012.10.037

D'Lima, D. D., Fregly, B. J., Patil, S., Steklov, N., & Colwell, C. W. (2012). Knee joint forces: Prediction, measurement, and significance. *Proceedings of the Institution of Mechanical Engineers, Part H: Journal of Engineering in Medicine*, *226*(2), 95–102. https://doi.org/10.1177/0954411911433372

Dolan, S. H., Williams, D. P., Ainsworth, B. E., Shaw, J. M., Williams, D. P., Ainsworth, B. E., & SHAW Development, J. M. (2006). Development and Reproducibility of the Bone Loading History Questionnaire. *Med. Sci. Sports Exerc*, *38*(6), 1121–1131. http://journals.lww.com/acsm-msse

Draghici, A. E., Picard, G., Taylor, J. A., & Shefelbine, S. J. (2017). Assessing kinematics and kinetics of functional electrical stimulation rowing. *Journal of Biomechanics*, *53*, 120–126. https://doi.org/10.1016/j.jbiomech.2017.01.007

Edwards, W. B., Schnitzer, T. J., & Troy, K. L. (2014). Bone mineral and stiffness loss at the distal femur and proximal tibia in acute spinal cord injury. *Osteoporosis International*, *25*(3), 1005–1015. https://doi.org/10.1007/s00198-013-2557-5

Edwards, W. B., Schnitzer, T. J., & Troy, K. L. (2013). Bone mineral loss at the proximal femur in acute spinal cord injury. *Osteoporosis International*, *24*(9), 2461–2469. https://doi.org/10.1007/s00198-013-2323-8

Edwards, W. B., & Schnitzer, T. J. (2015). Bone Imaging and Fracture Risk after Spinal Cord Injury. *Current Osteoporosis Reports*, *13*(5), 310–317. https://doi.org/10.1007/s11914-015-0288-6

Edwards, W. B., Schnitzer, T. J., & Troy, K. L. (2014). Reduction in proximal femoral strength in patients with acute spinal cord injury. *Journal of Bone and Mineral Research*, *29*(9), 2074–2079. https://doi.org/10.1002/jbmr.2227

Edwards, W. B., Simonian, N., Troy, K. L., & Schnitzer, T. J. (2015). Reduction in Torsional Stiffness and Strength at the Proximal Tibia as a Function of Time since Spinal Cord Injury. *Journal of Bone and Mineral Research*, *30*(8), 1422–1430. https://doi.org/10.1002/jbmr.2474

Eser, P., Frotzler, A., Zehnder, Y., Wick, L., Knecht, H., Denoth, J., & Schiessl, H. (2004). Relationship between the duration of paralysis and bone structure: A pQCT study of spinal cord injured individuals. *Bone*, *34*(5), 869–880. https://doi.org/10.1016/j.bone.2004.01.001

Fang, Y., Morse, L. R., Nguyen, N., Tsantes, N. G., & Troy, K. L. (2017). Anthropometric and biomechanical characteristics of body segments in persons with spinal cord injury. *Journal of Biomechanics*, *55*, 11–17. https://doi.org/10.1016/j.jbiomech.2017.01.036

Fang, Y., Troy, K. L., & Morse, L. (2021). Effect of Adapted Ergometer Setup and Rowing Speed on Lower Extremity Loading in People with and without Spinal Cord Injury. *Medrxiv*. https://doi.org/10.1101/2021.02.08.21251109

Faulkner, R., Forwood, M., Thomas, B., Mafukidze, J., Keith, R., & William, W. (2003). Strength indices of the proximal femur and shaft. *Medicine & Science in Sports & Exercise*, *35*(3), 513–518.

Franz-Odendaal, T. A., Hall, B. K., & Witten, P. E. (2006). Buried Alive: How Osteoblasts Become Osteocytes. *Developmental Dynamics*, *235*, 176–190. https://doi.org/10.1002/dvdy.20603

Frost, H. M. (1960). In Vivo Osteocyte Death. *Journal of Bone and Joint Surgery*, *42-A*(1), 138–143. https://doi.org/10.7868/s0869803114030138

Frotzler, A., Coupaud, S., Perret, C., Kakebeeke, T. H., Hunt, K. J., Donaldson, N. de N., & Eser, P. (2008). High-volume FES-cycling partially reverses bone loss in people with chronic spinal cord injury. *Bone*, *43*(1), 169–176. https://doi.org/10.1016/j.bone.2008.03.004

Garland, D. E., Adkins, R. H., Rah, A., & Stewart, C. A. (2001). Bone Loss with Aging and the Impact of SCI he body builds bone rapidly until the late teens and then continues at a slower rate in some locations until. In *Top Spinal Cord Inj Rehabil* (Vol. 6, Issue 3). http://meridian.allenpress.com/tscir/article-pdf/6/3/47/1984349/5w45-0l5b-8c7b-c93t.pdf

Garland, D. E., Adkins, R. H., & Stewart, C. A. (2008). Five-Year Longitudinal Bone Evaluations in Individuals With Chronic Complete Spinal Cord Injury. In *J Spinal Cord Med* (Vol. 31).

Gordon, K. E., Wald, M. J., & Schnitzer, T. J. (2013). Effect of parathyroid hormone combined with gait training on bone density and bone architecture in people with chronic spinal cord injury. *PM and R*, *5*(8), 663–671. https://doi.org/10.1016/j.pmrj.2013.03.032

Graeff, C., Campbell, G. M., Peña, J., Borggrefe, J., Padhi, D., Kaufman, A., Chang, S., Libanati, C., & Glüer, C. C. (2015). Administration of romosozumab improves vertebral trabecular and cortical bone as assessed with quantitative computed tomography and finite element analysis. *Bone*, *81*, 364–369. https://doi.org/10.1016/j.bone.2015.07.036

Hart, N. H., Nimphius, S., Rantalainen, T., Ireland, A., Siafarikas, A., & Newton, R. U. (2017). Mechanical basis of bone strength: influence of bone material, bone structure and muscle action. In *J Musculoskelet Neuronal Interact* (Vol. 17, Issue 3). http://www.ismni.org

Id, C. E., Padulle, J. M., Puig-divı, A., Marcos-ruiz, D., Busquets, A., & Padulle, X. (2019). Validity and reliability of the Kinovea program in obtaining angles and distances using coordinates in 4 perspectives. *PLOS One*, *Icc*, 1–14. https://doi.org/10.5281/zenodo.2843847

Jiang, S.-D., Li, A. E., Dai, -Yang, Lei, A. E., & Jiang, S. (2006). Osteoporosis after spinal cord injury. *Osteoporosis International*, *17*, 180–192. https://doi.org/10.1007/s00198-005-2028-8

Karelis, A. D., Carvalho, L. P., Castillo, M. J. E., Gagnon, D. H., & Aubertin-Leheudre, M. (2017). Effect on body composition and bone mineral density of walking with a robotic exoskeleton in adults with chronic spinal cord injury. *Journal of Rehabilitation Medicine*, *49*(1), 84–87. https://doi.org/10.2340/16501977-2173

Kazakia, G. J., Tjong, W., Nirody, J. A., Burghardt, A. J., Carballido-Gamio, J., Patsch, J. M., Link, T., Feeley, B. T., & Benjamin Ma, C. (2014). The influence of disuse on bone microstructure and mechanics assessed by HR-pQCT. *Bone*, *63*, 132–140. https://doi.org/10.1016/j.bone.2014.02.014

Lai, C. H., Chang, W. H. S., Chan, W. P., Peng, C. W., Shen, L. K., Chen, J. J. J., & Chen, S. C. (2010). Effects of functional electrical stimulation cycling exercise on bone mineral density loss in the early stages of spinal cord injury. *Journal of Rehabilitation Medicine*, *42*(2), 150–154. https://doi.org/10.2340/16501977-0499

Lambach, R. L., Stafford, N. E., Kolesar, J. A., Kiratli, B. J., Creasey, G. H., Gibbons, R. S., Andrews, B. J., & Beaupre, G. S. (2020). Bone changes in the lower limbs from participation in an FES rowing exercise program implemented within two years after traumatic spinal cord injury. *Journal of Spinal Cord Medicine*, *43*(3), 306–314. https://doi.org/10.1080/10790268.2018.1544879

Lang, T. F., Keyak, J. H., Heitz, M. W., Augat,', ' P, Lu, Y., Mathur,', A., Genant', H. K., & Lang, T. F. (1997). Volumetric Quantitative Computed Tomography of the Proximal Femur: Precision and Relation to Bone Strength. *Bone*, *21*(1), 101–108.

Lang, T. F., Leblanc, A. D., Evans, H. J., & Lu, Y. (2006). Adaptation of the proximal femur to skeletal reloading after long-duration spaceflight. *Journal of Bone and Mineral Research*, *21*(8), 1224–1230. https://doi.org/10.1359/jbmr.060509

Lang, T., LeBlanc, A., Evans, H., Lu, Y., Genant, H., & Yu, A. (2004). Cortical and trabecular bone mineral loss from the spine and hip in long-duration spaceflight. *Journal of Bone and Mineral Research*, *19*(6), 1006–1012. https://doi.org/10.1359/JBMR.040307

Lobos, S., Cooke, A., Simonett, G., Ho, C., Boyd, S. K., & Edwards, W. B. (2018). Assessment of Bone Mineral Density at the Distal Femur and the Proximal Tibia by Dual-Energy X-ray Absorptiometry in Individuals With Spinal Cord Injury: Precision of Protocol and Relation to Injury Duration. *Journal of Clinical Densitometry*, *21*(3), 338–346. https://doi.org/10.1016/j.jocd.2017.05.006

Maïmoun, L., Fattal, C., Micallef, J. P., Peruchon, E., & Rabischong, P. (2006). Bone loss in spinal cord-injured patients: From physiopathology to therapy. *Spinal Cord*, *44*(4), 203–210. https://doi.org/10.1038/sj.sc.3101832

Malone, A. M. D., Anderson, C. T., Tummala, P., Kwon, R. Y., Johnston, T. R., Stearns, T., Jacobs, C. R., & Lefkowitz, R. J. (2007). Primary cilia mediate mechanosensing in bone cells by a calcium-

independent mechanism. *Proceedings of the National Academy of Sciences of the United States of America*, *104*(33), 13325–13330. www.pnas.org/cgi/content/full/

Mancuso, M. E., Johnson, J. E., Ahmed, S. S., Butler, T. A., & Troy, K. L. (2018). Distal radius microstructure and finite element bone strain are related to site-specific mechanical loading and areal bone mineral density in premenopausal women. *Bone Reports*, *8*, 187–194. https://doi.org/10.1016/j.bonr.2018.04.001

Mekki, M., Delgado, A. D., Fry, A., Putrino, D., & Huang, V. (2018). Robotic Rehabilitation and Spinal Cord Injury: a Narrative Review. In *Neurotherapeutics* (Vol. 15, Issue 3, pp. 604–617). Springer New York LLC. https://doi.org/10.1007/s13311-018-0642-3

Mikic, B., & Carter, D. R. (1995). Technical note bone strain gage data and theoretical models of functional adaptation. *Journal of Biomechanics*, *28*(4), 465–469.

Modlesky, C. M., Majumdar, S., Narasimhan, A., & Dudley, G. A. (2004). Trabecular bone microarchitecture is deteriorated in men with spinal cord injury. *Journal of Bone and Mineral Research*, *19*(1), 48–55. https://doi.org/10.1359/JBMR.0301208

Mohamed, A. M. F. S. (2008). An overview of bone cells and their regulating factors of differentiation. In *Malaysian Journal of Medical Sciences* (Vol. 15, Issue 1, pp. 4–12). School of Medical Sciences, Universiti Sains Malaysia. /pmc/articles/PMC3341892/

Mohr, T., Pødenphant, J., Biering-Sørensen, F., Galbo, H., Thamsborg, G., & Kjaer, M. (1997). Increased Bone Mineral Density after Prolonged Electrically Induced Cycle Training of Paralyzed Limbs in Spinal Cord Injured Man. *Calcified Tissue International*, *61*(1), 22–25.

Moisio, K. C., Sumner, D. R., Shott, S., & Hurwitz, D. E. (2003). Normalization of joint moments during gait : a comparison of two techniques. *Journal of Biomechanics*, *36*, 599–603. https://doi.org/10.1016/S0021-9290(02)00433-5

Moran De Brito, C. M., Battistella, L. R., Saito, E. T., & Sakamoto, H. (2005). Effect of alendronate on bone mineral density in spinal cord injury patients: A pilot study. *Spinal Cord*, *43*(6), 341–348. https://doi.org/10.1038/sj.sc.3101725

Morse, L. R., Troy, K. L., Fang, Y., Nguyen, N., Battaglino, R., Goldstein, R. F., Gupta, R., & Taylor, J. A. (2019). Combination Therapy With Zoledronic Acid and FES-Row Training Mitigates Bone Loss in Paralyzed Legs: Results of a Randomized Comparative Clinical Trial. *JBMR Plus*, *3*(5). https://doi.org/10.1002/jbm4.10167

Morse, L. R., Biering-Soerensen, F., Carbone, L. D., Cervinka, T., Cirnigliaro, C. M., Johnston, T. E., Liu, N., Troy, K. L., Weaver, F. M., Shuhart, C., & Craven, B. C. (2019). Bone Mineral Density Testing in Spinal Cord Injury: 2019 ISCD Official Position. *Journal of Clinical Densitometry*, *22*(4), 554–566. https://doi.org/10.1016/j.jocd.2019.07.012

Nakashima, T., Hayashi, M., Fukunaga, T., Kurata, K., Oh-hora, M., Feng, J. Q., Bonewald, L. F., Kodama, T., Wutz, A., Wagner, E. F., Penninger, J. M., & Takayanagi, H. (2011). Evidence for osteocyte regulation of bone homeostasis through RANKL expression. *Nature Medicine*. https://doi.org/10.1038/nm.2452

Qiu, Z. Y., Cui, Y., & Wang, X. M. (2019). Natural bone tissue and its biomimetic. In *Mineralized Collagen Bone Graft Substitutes* (pp. 1–22). Elsevier. https://doi.org/10.1016/B978-0-08-102717-2.00001-1

Roberts, T. T., Leonard, G. R., & Cepela, D. J. (2017). Classifications In Brief: American Spinal Injury Association (ASIA) Impairment Scale. *Clinical Orthopaedics and Related Research*, *475*(5), 1499–1504. https://doi.org/10.1007/s11999-016-5133-4

Robling, A. G., Niziolek, P. J., Baldridge, L. A., Condon, K. W., Allen, M. R., Alam, I., Mantila, S. M., Gluhak-Heinrich, J., Bellido, T. M., Harris, S. E., & Turner, C. H. (2008). Mechanical stimulation of bone in vivo reduces osteocyte expression of Sost/sclerostin. *Journal of Biological Chemistry*, *283*(9), 5866–5875. https://doi.org/10.1074/jbc.M705092200

Robling, A. G., & Bonewald, L. F. (2020). *The Osteocyte: New Insights*. https://doi.org/10.1146/annurev-physiol-021119

Rodríguez-Fernández, A., Lobo-Prat, J., & Font-Llagunes, J. M. (2021). Systematic review on wearable lower-limb exoskeletons for gait training in neuromuscular impairments. In *Journal of NeuroEngineering and Rehabilitation* (Vol. 18, Issue 1). BioMed Central Ltd. https://doi.org/10.1186/s12984-021-00815-5

Schache, A. G., Blanch, P. D., Dorn, T. W., Brown, N. A. T., Rosemond, D., & Pandy, M. G. (2011). Effect of running speed on lower limb joint kinetics. *Medicine and Science in Sports and Exercise*, *43*(7), 1260–1271. https://doi.org/10.1249/MSS.0b013e3182084929

Shields, R. K., & Dudley-Javoroski, S. (2006). Musculoskeletal plasticity after acute spinal cord injury: Effects of long-term neuromuscular electrical stimulation training. *Journal of Neurophysiology*, *95*(4), 2380–2390. https://doi.org/10.1152/jn.01181.2005

Siu, W. S., Qin, L., & Leung, K. S. (2003). pQCT bone strength index may serve as a better predictor than bone mineral density for long bone breaking strength. *Journal of Bone and Mineral Metabolism*, *21*(5), 316–322. https://doi.org/10.1007/s00774-003-0427-5

Soleyman-Jahi, S., Yousefian, A., Maheronnaghsh, R., Shokraneh, F., Zadegan, S. A., Soltani, A., Hosseini, S. M., Vaccaro, A. R., & Rahimi-Movaghar, V. (2018). Evidence-based prevention and treatment of osteoporosis after spinal cord injury: a systematic review. In *European Spine Journal* (Vol. 27, Issue 8, pp. 1798–1814). Springer Verlag. https://doi.org/10.1007/s00586-017-5114-7

St. James, M. M., & Carroll, S. (2010). Effects of different impact exercise modalities on bone mineral density in premenopausal women: A meta-analysis. In *Journal of Bone and Mineral Metabolism* (Vol. 28, Issue 3, pp. 251–267). https://doi.org/10.1007/s00774-009-0139-6

Stagi, S., Cavalli, L., Cavalli, T., De Martino, M., & Brandi, M. L. (2016). Peripheral quantitative computed tomography (pQCT) for the assessment of bone strength in most of bone affecting conditions in developmental age: A review. In *Italian Journal of Pediatrics* (Vol. 42, Issue 1). BioMed Central Ltd. https://doi.org/10.1186/s13052-016-0297-9

Szollar, S. M., Martin, E. M. E., Parthemore, J. G., Sartoris, D. J., & Deftos, L. J. (1997). Densitometric patterns of spinal cord injury associated bone loss. *Spinal Cord*, 374–382.

Szollar, S. M., Martin, E., Sartoris, D., Parthemore, J., & Deftos, L. (1998). Bone mineral density and indexes of bone metabolism in spinal cord injury. *American Journal of Physical Medicine and Rehabilitation*, *77*(1), 28–35.

Talaty, M., Esquenazi, A., & Briceno, J. E. (2013). Differentiating ability in users of the ReWalkTM powered exoskeleton: An analysis of walking kinematics. *IEEE International Conference on Rehabilitation Robotics*. https://doi.org/10.1109/ICORR.2013.6650469

Troy, K. L., Mancuso, M. E., Johnson, J. E., Wu, Z., Schnitzer, T. J., & Butler, T. A. (2020). Bone Adaptation in Adult Women Is Related to Loading Dose: A 12-Month Randomized Controlled Trial. *Journal of Bone and Mineral Research*, *35*(7), 1300–1312. https://doi.org/10.1002/jbmr.3999

Troy, K. L., & Morse, L. R. (2015). Measurement of bone: Diagnosis of SCI-induced osteoporosis and fracture risk prediction. *Topics in Spinal Cord Injury Rehabilitation*, *21*(4), 267–274. https://doi.org/10.1310/sci2104-267

Tu, X., Rhee, Y., Condon, K. W., Bivi, N., Allen, M. R., Dwyer, D., Stolina, M., Turner, C. H., Robling, A. G., Plotkin, L. I., & Bellido, T. (2012). Sost downregulation and local Wnt signaling are required for the osteogenic response to mechanical loading. *Bone*, *50*(1), 209–217. https://doi.org/10.1016/j.bone.2011.10.025

Turner, C. H. (1998). Three rules for bone adaptation to mechanical stimuli. *Bone*, *23*(5), 399–407. https://doi.org/10.1016/S8756-3282(98)00118-5

Turner, C., & Robling, A. (2003). Designing Exercise Regimens to Increase Bone Strength. *Exercise and Sport Sciences Reviews*, *31*(1), 45–50.

Weeks, B. K., & Beck, B. R. (2008). The BPAQ: A bone-specific physical activity assessment instrument. *Osteoporosis International*, *19*(11), 1567–1577. https://doi.org/10.1007/s00198-008-0606-2

Winter, D. (2009). *Biomechanics and Motor Control of Human Movement*. John Wiley & Sons.

Zehnder, Y., Lüthi, M., Michel, D., Knecht, H., Perrelet, R., Neto, I., Kraenzlin, M., Zäch, G., & Lippuner, K. (2004). Long-term changes in bone metabolism, bone mineral density, quantitative ultrasound parameters, and fracture incidence after spinal cord injury: A cross-sectional observational study in 100 paraplegic men. *Osteoporosis International*, *15*(3), 180–189. https://doi.org/10.1007/s00198-003-1529-6

Zehnder, Y., Risi, S., Michel, D., Knecht, H., Perrelet, R., Kraenzlin, M., Zäch, G. A., & Lippuner, K. (2004). Prevention of bone loss in paraplegics over 2 years with alendronate. *Journal of Bone and Mineral Research*, *19*(7), 1067–1074. https://doi.org/10.1359/JBMR.040313

Zhao, W., Li, X., Peng, Y., Qin, Y., Pan, J., Li, J., Xu, A., Ominsky, M. S., Cardozo, C., Feng, J. Q., Ke, H. Z., Bauman, W. A., & Qin, W. (2018). Sclerostin Antibody Reverses the Severe Sublesional Bone Loss in Rats After Chronic Spinal Cord Injury. *Calcified Tissue International*, *103*(4), 443–454. https://doi.org/10.1007/s00223-018-0439-8